Circulation
Cardiovascular Genetics

Gene Network and Proteomic Analyses of Cardiac Responses to Pathological and Physiological Stress

Ignat Drozdov, Athanasios Didangelos, Xiaoke Yin, Anna Zampetaki, Mélanie Abonnenc, Colin Murdoch, Min Zhang, Christos A. Ouzounis, Manuel Mayr, Sophia Tsoka and Ajay M. Shah

Circ Cardiovasc Genet. 2013;6:588-597; originally published online November 8, 2013;
doi: 10.1161/CIRCGENETICS.113.000063
Circulation: Cardiovascular Genetics is published by the American Heart Association, 7272 Greenville Avenue, Dallas, TX 75231

Print ISSN: 1942-325X. Online ISSN: 1942-3268

Original Article

Gene Network and Proteomic Analyses of Cardiac Responses to Pathological and Physiological Stress

Ignat Drozdov, PhD; Athanasios Didangelos, PhD; Xiaoke Yin, PhD; Anna Zampetaki, PhD; Mélanie Abonnenc, PhD; Colin Murdoch, PhD; Min Zhang, PhD; Christos A. Ouzounis, PhD; Manuel Mayr, MD, PhD; Sophia Tsoka, PhD; Ajay M. Shah, MD, FMedSci

Background—The molecular mechanisms underlying similarities and differences between physiological and pathological left ventricular hypertrophy (LVH) are of intense interest. Most previous work involved targeted analysis of individual signaling pathways or screening of transcriptomic profiles. We developed a network biology approach using genomic and proteomic data to study the molecular patterns that distinguish pathological and physiological LVH.

Methods and Results—A network-based analysis using graph theory methods was undertaken on 127 genome-wide expression arrays of in vivo murine LVH. This revealed phenotype-specific pathological and physiological gene coexpression networks. Despite >1650 common genes in the 2 networks, network structure is significantly different. This is largely because of rewiring of genes that are differentially coexpressed in the 2 networks; this novel concept of differential wiring was further validated experimentally. Functional analysis of the rewired network revealed several distinct cellular pathways and gene sets. Deeper exploration was undertaken by targeted proteomic analysis of mitochondrial, myofilament, and extracellular subproteomes in pathological LVH. A notable finding was that mRNA–protein correlation was greater at the cellular pathway level than for individual loci.

Conclusions—This first combined gene network and proteomic analysis of LVH reveals novel insights into the integrated pathomechanisms that distinguish pathological versus physiological phenotypes. In particular, we identify differential gene wiring as a major distinguishing feature of these phenotypes. This approach provides a platform for the investigation of potentially novel pathways in LVH and offers a freely accessible protocol (http://sites.google.com/site/cardionetworks) for similar analyses in other cardiovascular diseases. **(*Circ Cardiovasc Genet*. 2013;6:588-597.)**

Key Words: computational biology ■ genetics ■ genomics ■ proteomics

Hearts under chronic hemodynamic disease stress develop pathological left ventricular hypertrophy (LVH), a complex remodeling response that predisposes to heart failure.[1] Pathological remodeling is associated with interstitial fibrosis, cardiomyocyte apoptosis, contractile dysfunction, and arrhythmia.[2] The heart also remodels with chronic exercise or pregnancy, but such physiological LVH is unaccompanied by fibrosis, apoptosis, or significant contractile dysfunction and carries no risk of failure.[3] Delineation of the molecular mechanisms driving these divergent responses may inform therapeutic strategies for pathological LVH and heart failure. Much work has focused on targeted investigation of specific signaling pathways in the pathogenesis of physiological or pathological LVH and revealed novel insights.[1] However, few novel therapies have emerged, and complementary approaches for target discovery need to be considered.[4]

Clinical Perspective on p 597

Network-based analyses of disease phenotypes involve systems-level characterization of biological mechanisms to uncover the complex relationships between genes or proteins and their environment.[5] Analysis of the functional architecture of gene and protein networks that orchestrate disease development might provide a useful foundation for novel therapeutic approaches.[6] Indeed, such approaches have begun to yield positive results in areas such as oncology,[7] but have only recently been applied to cardiac disease.[8,9] Previous studies used microarray experiments to explore gene expression differences in cardiac hypertrophy.[10] Such studies reported that genes associated with pathological hypertrophy included inflammatory, apoptotic, fetal reprogramming, and oxidative stress pathways whereas genes associated with physiological hypertrophy affected metabolism and insulin signaling.[11]

Received February 12, 2013; accepted October 30, 2013.

From the Cardiovascular Division, King's College London BHF Centre of Research Excellence, School of Medicine, James Black Centre, London, United Kingdom (I.D., A.D., X.Y., A.Z., M.A., C.M., M.Z., M.M., A.M.S.); and Department of Informatics, School of Natural and Mathematical Sciences, King's College London, London, United Kingdom (I.D., C.A.O., S.T.). Current address for C.A.O.: Computational Genomics Unit, Institute of Applied Biosciences, Centre for Research & Technology Hellas, Thessalonica, Greece, and Donnelly Centre for Cellular & Biomolecular Research, University of Toronto, Toronto, Ontario, Canada.

The online-only Data Supplement is available at http://circgenetics.ahajournals.org/lookup/suppl/doi:10.1161/CIRCGENETICS.113.000063/-/DC1.

Correspondence to Ajay M. Shah, MD, King's College London, James Black Centre, Denmark Hill Campus, 125 Coldharbour Ln, London SE5 9NU, United Kingdom. E-mail ajay.shah@kcl.ac.uk

However, a global framework of the mechanisms driving similarities and differences between these phenotypes is lacking.

We developed a network-based genomic and proteomic framework for comparing gene coexpression networks underlying pathological and physiological LVH. Comprehensive characterization of network properties allowed us to identify that a large number of genes were differentially wired in pathological LVH. Integration of transcriptomic data of pathological LVH with a proteomic analysis of mitochondrial, myofilament, and extracellular subproteomes allowed the establishment of gene–protein relationships for individual loci and entire pathways. This comprehensive analysis at transcriptome and proteome levels reveals novel insights into the molecular basis of pathological versus physiological LVH and provides a resource for further studies of genotype–phenotype relationships in this condition.

Methods

Detailed methods are provided in the online-only Data Supplement.

Gene Expression Analysis

Six mouse microarray data sets (n=127 arrays) were obtained from ArrayExpress (Table 1).[12] Raw gene expression was processed using robust multi-array average, and each array was inspected for outlying samples. Affymetrix probe identifiers were mapped to corresponding Entrez gene identifiers.[13]

Graph Theory Methods

Reverse Engineering Gene Coexpression Networks

Gene coexpression networks were reconstructed by expressing pairwise similarity in expression profiles by the Pearson correlation coefficient (PCC). Gene pairs that correlated above a predefined PCC threshold were represented as an undirected unweighted network, where nodes correspond to genes and links (edges) correspond to coexpression between genes. We used a data-driven computational method to calculate the appropriate PCC threshold for each microarray data set.

Network Topology

Node degree denotes the number of links a node has to other nodes. Nodes with high degree in biological networks (or hubs) are reported to be essential for processes such as cell survival.[14] Betweenness centrality is the number of shortest paths that pass through a node. Nodes with the highest betweenness represent the critical points of information flow within a network. Eigenvector centrality is a measure of overall network connectivity, denoting connections of nodes to other nodes that are central within the network. Clustering coefficient represents the number of node neighbors that are also interconnected. In protein–protein interaction networks, genes harboring disease-causing mutations tend to be distant from dense-clustering neighborhoods.[15] The shortest path is the shortest distance connecting any 2 genes. The diameter is the longest short path between any pair of genes in the network.

Gene Rewiring

The number of connections of each gene (node degree) was scaled to a value between 0 and 1 by dividing each node degree by the largest degree in a network. Differential wiring of genes common to pathological and physiological networks was computed by subtracting the node degree in the physiological network from node degree in the pathological network.[16] Thus, genes with positive rewiring are more central in the pathological network compared with physiological network.

Animal Studies

Procedures were performed in accordance with the Guidance on the Operation of the Animals (Scientific Procedures) Act, 1986 (United Kingdom). Aortic constriction (AC) and running exercise were performed as described.[17,18]

Reverse Transcription Polymerase Chain Reaction

RNA was isolated from 22 mouse LV samples (wild type [WT]-sham: n=6; AC: n=6; WT-sedentary: n=5; WT-running: n=5). Transcript expression was quantified using TaqMan probes (Applied Biosystems).

Nanoflow Liquid Chromatography–Tandem Mass Spectrometry

Liquid chromatography–tandem mass spectrometry analyses of LVs from 4 WT sham-operated mice, 4 angiotensin II–induced hypertrophy, and 4 LVs after AC were performed as

Table 1. Murine Cardiac Hypertrophy Data Sets Used for Reconstruction of Coexpression Networks

Data Set	Description	ArrayExpress	Nodes	Edges	Degree	Clustering Coefficient
AC1	Male, time series AC (n=18)	E-MEXP-105	8688	1 514 278	348.6	0.29
AC2	Sham and AC (n=34)	E-GEOD-76	8688	3 272 821	753.4	0.40
AT1	Wild type; cardiac-specific AT1 receptor overexpression (n=16)	E-GEOD-2355	8688	1 303 988	300.1	0.28
Akt	Wild type; short-term cardiac-specific Akt1 overexpression (n=18)	E-GEOD-3383	8688	1 404 578	327.4	0.29
PI3K	Wild type; cardiac-specific caPI3K or dnPI3K overexpression (n=9)	E-GEOD-558	8579	1 565 558	364.9	0.33
Swimming	Wild type; short-term exercise; long-term exercise (n=29)	E-GEOD-77	8579	2 367 500	551.9	0.35
Pathological	Consensus pathological hypertrophy network	N/A	3634	13 558	7.5	0.11
Physiological	Consensus physiological hypertrophy network	N/A	3156	4486	2.8	0.06

AC indicates aortic constriction; AT, angiotensin II receptor type 1; caPI3K, constitutively active phosphatidylinositol 3-kinase; dnPI3K, dominant-negative phosphatidylinositol 3-kinase; and N/A, not applicable.

described,[19] with modifications. We used a novel protocol that enriches extracellular matrix (ECM)[19] and myofilament[20] proteins (Methods in the online-only Data Supplement).

Statistical Analysis

Differential expression analysis was performed by fitting a linear model with empirical Bayes shrinkage to the log intensities of expression values for each gene.[21] *P* values were adjusted to control the expected false discovery rate using Benjamini–Hochberg correction. False discovery rate–controlled values of $P<0.05$ were considered significant.

Results

Construction of the LVH Networks

After data preprocessing and outlier removal (Methods in the online-only Data Supplement), our analysis included 124 samples from 6 mouse microarray data sets in different models of pathological and physiological LVH (Table 1). For each data set, we created a gene coexpression matrix of pairwise PCC (Figure I in the online-only Data Supplement). Only gene pairs with significant coexpressions were considered. Because all LVH networks contained a large number of edges (≤3.3 million; Table 1), nodes and edges that may arise because of experimental variability were filtered through intersection of networks. The intersection of the 3 pathological networks contained 3634 genes and 13 558 links (pathological, Tables I and III in the online-only Data Supplement) whereas the intersection of the 3 physiological networks produced comparable numbers, namely, 3156 genes and 4486 links (physiological, Tables II and IV in the online-only Data Supplement; Figure 1A). These intersections were compared against a random background by shuffling edges in the original networks 200× while preserving their degrees and then calculating their intersections. Intersections of randomized pathological and physiological hypertrophy networks contained an average of 3882.9 (SD=91.2) and 3312.6 (SD=77.7) links, respectively. Thus, the identification of 13 558 and 4486 conserved coexpressions in the real pathological and physiological networks was considered a nonrandom instance against the simulated background (*z* score=106.13 and 15.1, respectively; Figure 1A–1D).

Hypertrophy Networks Are Phenotype Specific

We tested the phenotype specificity of the pathological and physiological networks by enriching the gene sets for established mouse mutant phenotypes using the MamPhEA tool.[22] Pathological network genes were enriched for phenotypes including cardiovascular system phenotype (adjusted $P=1.6\times10^{-7}$), prenatal lethality (adjusted $P=2.9\times10^{-6}$), abnormal cardiovascular system morphology (adjusted $P=5.3\times10^{-6}$), and abnormal blood vessel morphology (adjusted $P=5.7\times10^{-4}$) whereas physiological network genes were enriched primarily for prenatal lethality ($P=4.9\times10^{-6}$; Figure 2A and 2B). Thus, the derived gene networks obtained through computational integration of the microarray expression data reflect the cardiovascular phenotype.

We examined whether the genes contributing to the cardiovascular phenotype are more connected than other genes in the pathological and physiological networks. We identified 19

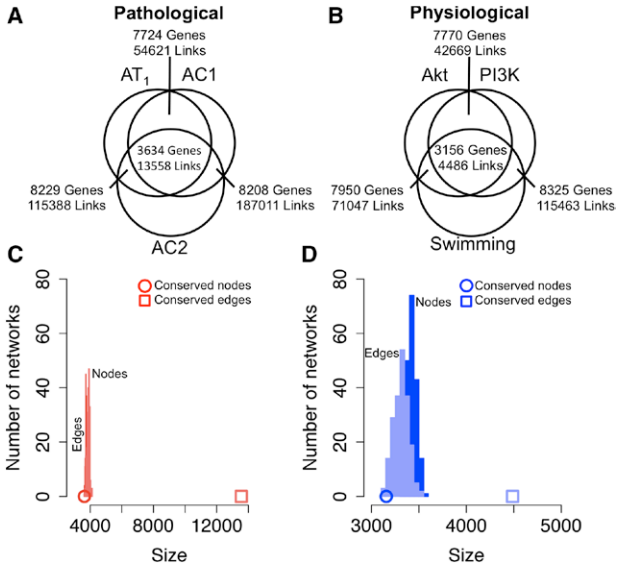

Figure 1. Genome-wide transcriptional networks in pathological and physiological hypertrophy. **A** and **B**, Venn diagrams of common nodes and coexpressions in pathological and physiological hypertrophy networks. Pathological and physiological networks reflect intersections of all hypertrophic interactomes. **C** and **D**, Frequency histograms comparing sizes of the pathological and physiological networks (denoted by conserved nodes and edges) with randomly generated networks with preserved node degree distributions. The *x* axis represents number of nodes or edges whereas the *y* axis represents number of networks. AC indicates aortic constriction; AT, angiotensin II receptor type 1; and PI3K, phosphatidylinositol 3-kinase.

and 6 layers of differential connectivity in the pathological and physiological networks, respectively, by peeling[23] each gene network (Methods in the online-only Data Supplement). These layers reflect gene connectivity neighborhoods such that the first peeled layer contains genes with only a few connections whereas the last layer contains the most connected genes (Figure II in the online-only Data Supplement). Interestingly, pathological network cardiovascular genes (≈22%) localized to the intermediate (layers 9–10) but not dense layers (Figure 2C). Conversely, physiological network cardiovascular genes localized to the densest layers (Figure 2D). This structural property of cardiovascular genes in the context of LVH phenotypes may be used to identify additional genes involved in cardiac function.[24]

Next, we expanded the functional characterization of coexpressed genes using enrichment analysis of genes that appear only in pathological (n=1980) or physiological (n=1502) network. The pathological-specific group had a predominance of genes involved in metabolic, apoptotic, and energy production processes, with subcellular localization to mitochondria and extracellular region. In contrast, physiological-specific genes were involved in processes including angiogenesis and cell cycle (Table V in the online-only Data Supplement). Similar enrichment analysis for all pathological and physiological network genes is shown in Table VI in the online-only Data Supplement.

Topological Properties of Gene Networks

We first assessed the stability of the pathological and physiological networks to targeted removal of hubs (simulated attack)

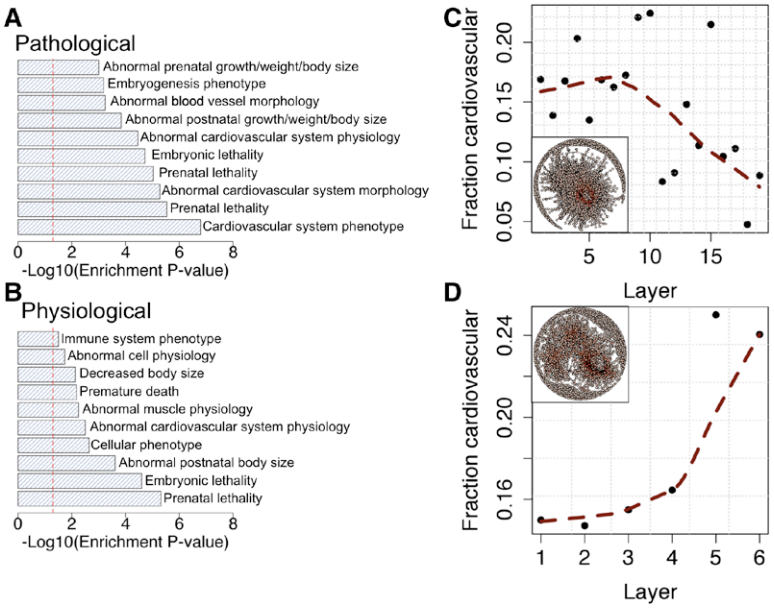

Figure 2. Phenotype specificity of the pathological and physiological left ventricular hypertrophy networks. **A** and **B**, MamPhEA-driven enrichment of genes specific to the pathological and physiological networks for phenotypes associated with mutations in these genes. Vertical red lines indicate adjusted P =0.05. **C** and **D**, Relationships between gene coexpression layers and frequency of gene implicated in cardiovascular phenotypes identified in each layer. Increasing layer numbers correspond to regions of increasing densities in the network. Inset graphs visualize pathological and physiological gene coexpression network, with darker node colors reflecting higher gene connection densities. Dotted lines represent locally weighted scatter plot smoothing fit.

or random nodes (simulated error).[25] Although removal of hubs (attack) had little effect on the pathological network, the physiological network rapidly collapsed into smaller subnetworks, reflected by increasing network diameter (Figure 3A). This suggests an unexpected level of robustness of gene coexpressions in the pathological network. Removal of random genes (error) had no effect on either network diameter (Figure 3A).

Comparison of global topologies demonstrated that the pathological network is denser than the physiological network (density 0.002 versus 0.0009), with a lower network diameter (20 versus 25). Local topological properties of the networks are shown in Figure 3A–3F and listed in Tables III and IV in the online-only Data Supplement. Overall, the pathological network had a larger average node degree (7.5 versus 2.8), eigencentrality (0.03 versus 0.01), and clustering coefficient (0.11 versus 0.06) but smaller betweenness (5921.8 versus 6573) and average shortest path length (5.7 versus 9.2; Figure 3A–3F). This topological comparison suggests that the genes under pathological stress form more coexpression links, yielding a dense and robust network. This phenomenon could reflect tight transcriptional regulation under pathological conditions.[26]

Identification of Gene Rewiring

When the pathological and physiological networks were compared on a coexpression level, 1654 (46%) of 3634 genes in the pathological network were also present in the physiological network. However, despite this large number of common genes, the 2 networks shared only 60 coexpression links (Figure III in the online-only Data Supplement). We further assessed topological overlap between pathological and physiological networks at the gene community level. For each network, gene communities were identified by

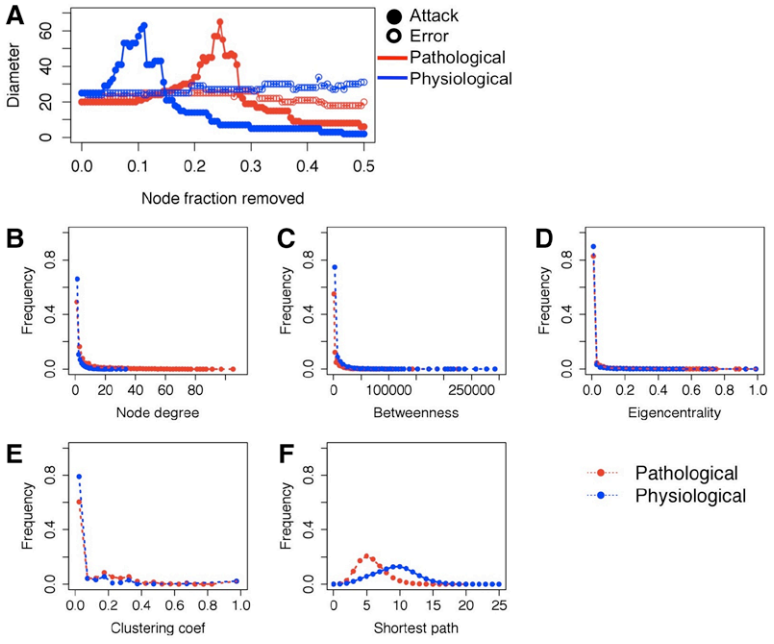

Figure 3. Topology of the pathological and physiological networks. **A**, Network diameter as a function of number of genes removed from the pathological and physiological networks. Removal of hubs (most connected genes) is labeled as attack whereas removal of random nodes is labeled as error. **B** to **F**, Frequency distributions of gene topologies in the pathological and physiological networks.

optimizing network modularity (Methods in the online-only Data Supplement).[23] Similarity between gene communities was expressed using Jaccard coefficient, computed as a ratio of the number of common genes in any 2 pathological and physiological network communities to the total number of genes in these communities. Disparate and identical communities would correspond to Jaccard coefficient of 0 and 1, respectively. On average, Jaccard coefficient for 350 and 411 communities in the pathological and physiological networks, respectively, was 0.0002. Therefore, pathological and physiological networks do not share common topologies at either individual gene coexpression level or gene community level. Most of the shared coexpressions were between genes encoding ECM proteins (eg, *Col1a1*, *Col4a1*, *Col5a2*, *Col6a2*, and *Serpinf1*).

Because of the low frequency of common coexpressions between pathological and physiological networks, it is likely that a significant subset of hypertrophy-associated genes is subject to differential coexpression, or rewiring, in response to pathological stress. Consequently, differentially wired genes may contribute to phenotypic differences between pathological and physiological LVH. To construct the rewired network, subnetworks consisting of 1654 genes shared by the pathological and physiological interactomes were extracted and then merged. Because several genes were singletons (single nodes without additional coexpressions), the rewired network was reduced to 1553 genes connected by 6197 links (Figure 4A).

For each rewired gene, we calculated a differential wiring score (see Methods; Figure 4B). A score >0 indicates that a gene is more connected in the pathological network whereas a score <0 indicates greater connectivity in the physiological network. Overall, 539 and 1014 genes had positive and negative differential wiring scores, respectively (Table VII in the online-only Data Supplement). Other parameters of local network topology (eg, betweenness centrality) are also reported in Table VII in the online-only Data Supplement.

Experimental Validation of Differentially Wired Genes

Gene rewiring can be interpreted as acquisition or loss of coexpression links in a stimulus-dependent manner. This is a direct consequence of changes in gene expression. To experimentally validate implication of differentially wired genes in LVH phenotypes, we used quantitative polymerase chain reaction to measure expression profiles of 10 rewired genes, namely, *Col1a1*, *Col4a1*, *Col5a2*, *Paip2b*, *Phtf2*, *Prps1*, *Rnf14*, *Serpinh1*, *Sparc*, and *Tiprl* (Table 2), in mouse models of pathological (AC, n=6) and physiological (treadmill, n=6) LVH and corresponding controls (WT-sham, n=5; WT-sedentary, n=5; Figure IV in the online-only Data Supplement). These genes were selected to reflect diverse ranges of differential wiring, and their respective fold changes in the microarray were not considered (Figure 4B; Table 2). Differential expression analysis confirmed that all transcripts, with the exception of *Rnf14*, were significantly changed in AC compared with sham-operated controls (4 downregulated, 5 upregulated; $P<0.05$; Table 3; Figure 4C). Indeed, *Rnf14* had a low degree of rewiring of −0.002. Importantly, none of the transcripts was differentially expressed in physiological LVH compared with WT hearts (Figure 4C), which is consistent with our computational evidence of rewiring in manifestation of pathological LVH.

Functional Characteristics of Rewired Genes

Given that differentially wired genes may reflect potentially important contributors to the pathological LVH phenotype, we further analyzed these genes. Using gene mutation information from the Mouse Genome Informatics database, it was

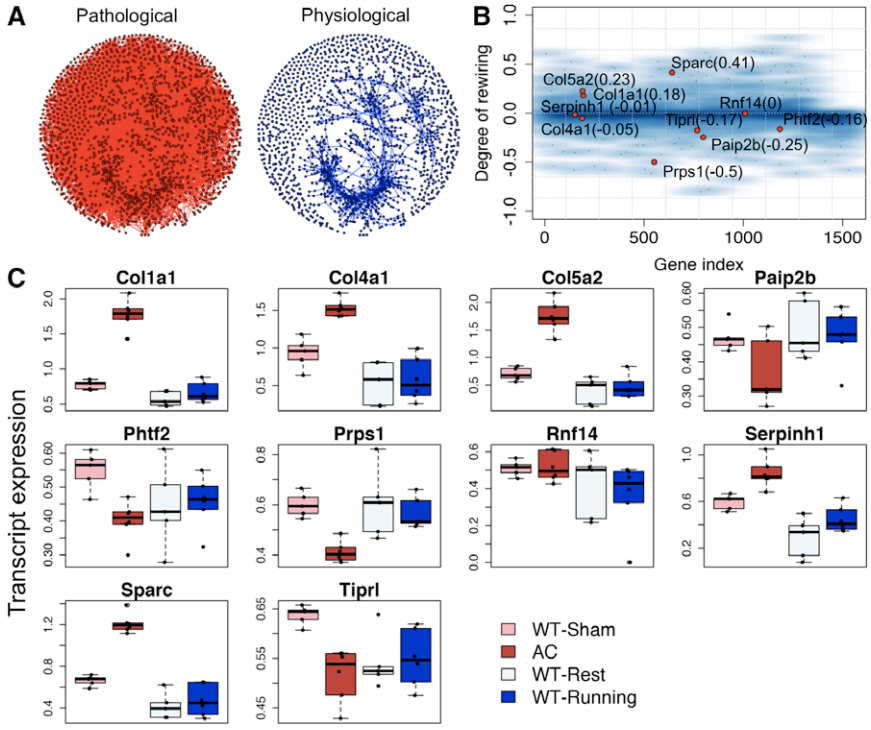

Figure 4. Rewiring of hypertrophy gene networks. **A**, The rewired network consisting of 1553 genes. Nodes indicate genes whereas red and blue edges correspond to pathological and physiological coexpressions, respectively. Node positions in each plot are kept constant to facilitate visualization of rewired coexpressions. **B**, Density map of differential wiring scores (*y* axis) for 1553 genes (*x* axis). Darker colors correspond to increased point density. Red points indicate the 10 rewired genes selected for further validation, with rewiring scores given in parentheses. **C**, Box plots visualizing quantitative polymerase chain reaction validation of 10 rewired genes. The *y* axis reflects GAPDH-normalized transcript expression values.

Table 2. Quantitative Polymerase Chain Reaction Validation of Rewired Genes

Symbol	Name	Function	Rewiring	Fold Change (AC vs Sham)	*P* Value (AC vs Sham)
Col1a1	Collagen, type I, α 1	Collagen biosynthesis	0.18	1	9.90×10^{-10}
Col4a1	Collagen, type IV, α 1	Collagen biosynthesis	−0.05	0.6	4.50×10^{-4}
Col5a2	Collagen, type VI, α 2	Collagen biosynthesis	0.23	1.04	2.00×10^{-7}
Paip2b	Poly(A)-binding protein–interacting protein 2B	Translation repressor activity	−0.25	−0.11	0.0499
Phtf2	Putative homeodomain transcription factor 2	DNA binding	−0.16	−0.15	0.0114
Prps1	Phosphoribosyl pyrophosphate synthetase 1	Nucleotide synthesis	−0.5	−0.19	0.0025
Rnf14	Ring finger protein 14	Transcription coactivator activity	0	0.006	0.938
Serpinh1	Serpin peptidase inhibitor, clade H (heat shock protein 47), member 1	Stress response	−0.01	0.25	0.0046
Sparc	Osteonectin	Collagen binding	0.41	0.55	2.00×10^{-7}
Tiprl	TIP41, TOR signaling pathway regulator-like	DNA damage checkpoint	−0.17	−0.12	0.0051

AC indicates aortic constriction; and Paip2b, poly(A)-binding protein–interacting protein 2B.

noted that the rewired network included 241 (16%) genes in which null mutations result in cardiac phenotypes (eg, interleukin-1 receptor-associated kinase 1, superoxide dismutase, and vascular endothelial growth factor B). In addition, cardiovascular system phenotype and abnormal cardiovascular morphology were the most enriched phenotypes (adjusted $P=6.3\times10^{-4}$ and 1.9×10^{-3}; Figure V in the online-only Data Supplement). Gene set enrichment of all rewired genes for Reactome pathways, as well as gene ontology biological process and gene ontology cellular component terms, revealed several distinct functional groups (Table 3), including major histocompatibility complex class II antigen presentation and tricarboxylic acid cycle and respiratory electron transport pathways with cellular localization to ECM, mitochondrial part, and stress fiber.

Functional enrichment of genes in the top 25th percentile of differential wiring (n=388 genes) identified gene ontology biological process terms such as hydrogen peroxide metabolic process and positive regulation of macroautophagy (Table VIII in the online-only Data Supplement). Interestingly, genes in the bottom 25th percentile of differential wiring were not significantly enriched.

Table 3. Top 10 Most Enriched Functional Terms in the Rewired Network

Reactome		GO-BP		GO-CC			
Term	Estimate	Genes	Term	Estimate	Genes	Term	Estimate	Genes
MHC class II antigen presentation	0.98	21	Regulation of RNA splicing	0.82	21	Extracellular matrix	0.92	40
TCA cycle and respiratory electron transport	0.96	37	Response to metal ion	0.77	37	Cytosol	0.74	138
Mitochondrial protein import	0.78	11	Protein heterooligomerization	0.75	11	Spliceosomal complex	0.72	20
Developmental biology	0.74	66	Energy derivation by oxidation of organic compounds	0.46	66	Mitochondrial part	0.71	86
Interferon signaling (REACT_127785.1)	0.64	14	Coenzyme metabolic process	0.26	14	Extrinsic to plasma membrane	0.62	17
Platelet degranulation	0.64	21	Nucleoside triphosphate metabolic process	0.24	21	Postsynaptic membrane	0.41	16
Amino acid and derivative metabolism	0.59	41	Generation of precursor metabolites and energy	0.22	41	Stress fiber	0.32	12
Circadian clock	0.57	13	Regulation of wound healing	0.21	13	COPI-coated vesicle	0.28	6
Cytosolic tRNA aminoacylation	0.49	8	Hydrogen peroxide metabolic process	0.17	8	Actomyosin	0.27	13
Generic transcription pathway	0.45	23	Negative regulation of cellular component organization	0.16	23	Soluble fraction	0.27	49

Estimate indicates the posterior probability of term enrichment, whereby most enriched terms will be characterized by high probability estimate values; GO-BP, gene ontology biological process; GO-CC, gene ontology cellular component; MHC, major histocompatibility complex; and TCA, tricarboxylic acid cycle.

Analysis of the Extracellular and Myofilament Proteomes in Pathological LVH

The above computational analysis and quantitative polymerase chain reaction validation suggest that genes localized to the ECM and myofilaments, among others, are differentially wired in pathological LVH. Thus, we further explored these findings using a proteomic approach. LVs were obtained from 2 murine models of pathological hypertrophy—angiotensin II infusion (n=4) and AC (n=4)—and sham-operated controls (n=4). To enable a better characterization of myofilament and ECM proteins, we enriched for these subproteomes using solubility-based protein subfractionation methodologies (see Methods in the online-only Data Supplement).[19,20] Western blotting of the subfractions confirmed that the extracts were rich in myofilament (eg, troponin I type 3 [TNNI3_MOUSE]) and extracellular proteins (eg, collagen α-2 [VI] [CO6A2_MOUSE], glutathione peroxidase 3) whereas membrane and cytosolic proteins (eg, ITA8_MOUSE, β-actin [ACTB_MOUSE]) were depleted (Figure 5A). Subsequently, the enriched extracts were separated by SDS-PAGE, subjected to in-gel tryptic digestion, and analyzed by liquid chromatography–tandem mass spectrometry (see Methods). Two complementary approaches, spectral counting and peptide ion intensities, were used to estimate protein abundance. Quantitative information is available from both methods, which produced comparable results (Figure VI and Data Sets I and II in the online-only Data Supplement). For subsequent analysis, we focused on spectral counting–based quantification, given its greater dynamic range than peptide ion intensities (2268 versus 385 proteins).

Principal component analysis of 1300 proteins that passed filtering criteria (Methods in the online-only Data Supplement) in the proteomic data revealed a separation of sham-operated controls and hypertrophic samples (Figure 5B). Enrichment of 1300 proteins for gene ontology cellular component terms confirmed successful enrichment for myofilament (n=68) and extracellular (n=100) proteins in the extracted subproteome. In addition, mitochondrial proteins were also detected (n=292; Figure 5C). Spectral count information for the different subproteomes is visualized in Figure 5D and listed in Table IX in the online-only Data Supplement. Overall, 12 of 30 (40%), 80 of 226 (35%), and 22 of 102 (22%) rewired genes that were predicted to be myofilament, mitochondrial, and extracellular were also quantified by proteomics.

To define the relationship between changes in gene expression and protein levels, we correlated protein and mRNA expression ratios using PCC. We used the pathological microarray cohort (AC1, AC2, angiotensin II receptor type 1 data sets; Table 1) to identify 2796 mRNAs with consistent changes compared with controls across all data sets. Similarly, we identified 170 proteins with consistent changes in AC and angiotensin subproteomes compared with sham-operated mice. Subsequently, 170 protein–transcript pairs were compared using respective fold changes compared with normal, revealing a significant but relatively modest positive correlation between the proteomic and transcriptomic changes (PCC=0.25; P=0.0008; Figure 6A). Although the spectral counts of the mitochondrial subproteome did not correlate with mRNA expression (PCC=–0.19; P=0.11), myofilament and extracellular subproteomes showed stronger positive correlation (PCC=0.52; P=0.16 and PCC=0.56; P=0.03, respectively; Figures 6A). Quantitative information for mRNA–protein relationships is listed in Table X in the online-only Data Supplement. Furthermore, we calculated average fold changes of mRNAs and proteins that mapped to unique Reactome[27] pathways (289

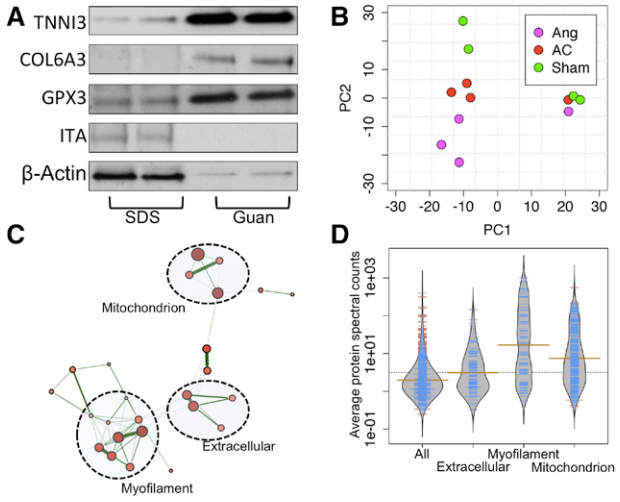

Figure 5. Proteomic profiling of pathological cardiac hypertrophy. **A**, Validation of the solubility-based protein subfractionation methodology in sham-operated hearts. The 4 mol/L guanidine fraction (Guan) is enriched for myofilament and extracellular proteins whereas membrane and cytosolic proteins are depleted. **B**, Principal component analysis (PCA) of 1300 proteins separated control hearts from angiotensin (Ang)- and aortic constriction (AC)–induced cardiac hypertrophy. **C**, Network-based visualization of functional enrichment of 764 proteins for gene ontology (GO) cellular process. Each node represents a GO-cellular component (CC) term whereas a link represents shared proteins between terms. Analysis was performed using Enrichment Map tool (see Material in the online-only Data Supplement). **D**, Bean plots reflecting distributions of the average (thick horizontal line) spectral counts of mitochondrial, myofilament, and extracellular proteins in the Guan extract. GPX3 indicates glutathione peroxidase 3; ITA, integrin-alpha8; PC, principal component; and TNNI3, troponin I type 3.

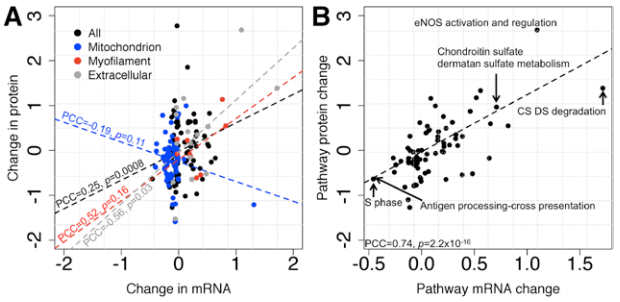

Figure 6. Correlation profiles of protein and mRNA changes in pathological cardiac hypertrophy. **A**, Scatter plot of changes in protein and transcript abundance (assessed using the t value of respective spectral counts) consisting of 170 protein–transcript pairs. Correlation was measured using the Pearson correlation coefficient. **B**, Correlation of mRNA and protein expressions across 289 Reactome pathway components (Table IX in the online-only Data Supplement). For each pathway that was identified in the pathological hypertrophy data set, the average mRNA and corresponding protein expression ratios were determined and plotted. CS DS indicates chondroitin sulfate dermatan sulfate; eNOS, endothelial nitric oxide synthase; and PCC, Pearson correlation coefficient.

pathways represented by 631 mRNA–protein pairs). When considered the Reactome pathway level, mRNA–protein correlation was much stronger (PCC=0.74; $P=2.2\times10^{-16}$) and across upregulated pathways such as chondroitin sulfate dermatan sulfate metabolism, chondroitin sulfate and dermatan sulfate degradation, and endothelial nitric oxide synthase activation and regulation and downregulated pathways, including S phase and antigen processing-cross presentation (Figure 6B; Table XI in the online-only Data Supplement).

Discussion

We used a combined gene network and proteomic approach to characterize pathological and physiological LVH phenotypes on a systems-wide level. This analysis shows that pathological and physiological network topologies are significantly different, with the notable finding that there is differential gene wiring in pathological versus physiological stress. This coexpression rewiring captures differences in metabolic and energy production processes, contractile fibril organization, and ECM turnover, being highly consistent with the phenotype studied. Furthermore, many of these pathways were experimentally explored at the proteome level. This network biology approach contributes novel insights into the integrated mechanisms of pathological LVH and heart failure.

Cardiac Gene Networks

Several studies have compared gene expression profiles in pathological and physiological LVH using microarray experiments.[28] However, there seems to be a large discrepancy in the number of genes and types of signaling pathways reported for these phenotypes. One reason may be variability in statistical prioritization of significantly regulated genes.[29] Thus, a comprehensive network-based meta-analysis of cardiac transcriptomes as presented here has advantages compared with conventional statistical approaches (eg, *t* test or ANOVA). In this study, we included relevant transcript expression data sets with multiple replicates to reduce noise. We also used an automated method for reverse engineering coexpression networks, thus eliminating selection bias typically associated with conventional statistical analysis of differential expression. Importantly, our data were combined at the level of correlation matrices rather than gene expression levels, which facilitates between-study comparisons and improves functional relevance of identified coexpressed genes.[30] Functional enrichment of the pathological and physiological networks revealed significant over-representation of genes implicated in cardiovascular system phenotypes and features consistent with previous studies that reported altered fatty acid metabolism, cellular apoptosis, sarcomeric organization, and protein synthesis in pathological LVH[31] and upregulation of cell survival, autophagy, and angiogenesis in physiological LVH.[11] These findings suggest that gene network profiling captures the underlying biology of hypertrophy phenotypes.

Evaluation of gene connectivity patterns (ie, network topology) provides additional insights into organizational principles of gene networks. Compared with the physiological network, the pathological LVH network was characterized by shorter average path length and higher average node degree. Although the connectivity of either pathological or physiological network was unaffected by removal of random genes, the physiological interactome collapsed in response to the removal of hub genes whereas the pathological network remained intact. These findings suggest that under pathological stress, genes have considerably more coexpression links than under physiological stress. Biologically, this may reflect differences in transcriptional regulation between LVH phenotypes.[26] Recently, Dewey et al[8] undertook a gene coexpression network analysis of pathological LVH, focusing on the extent of recapitulation of fetal gene expression programs, and could identify specific modules active during both development and disease. In contrast to that study and our previous coexpression analysis of LVH,[32] in the current work, a major focus was the differential network topology comparison of pathological versus physiological LVH. The current analysis reveals that a substantial number of genes (1553) are differentially wired in pathological compared with physiological LVH. Furthermore, several functional groups of rewired genes could be identified, including those involved in electron transport, myofilament organization, and ECM remodeling. Conceptually, gene rewiring can be regarded as the acquisition or loss of coexpression links in a stimulus-dependent manner. Therefore, rewiring is a direct result of changes in expression within the network. We experimentally validated the rewiring of 10 genes involved in ECM organization (*Col1a1*, *Col4a1*, *Col5a2*, *Sparc*), stress response (*Serpinh1*), and transcription and translation (*Paip2b*, *Phtf2*, *Prps1*, *Rnf14*, *Tiprl*) by confirming differential transcript expression of all rewired genes in pathological but not exercise models of cardiac hypertrophy. In addition, we observed no differential expression for *Rnf14*, a poorly rewired transcript. The functional groups of rewired genes that have been identified (Table 3) include those known to be involved in pathological LVH (eg, ECM genes, tricarboxylic acid cycle cycle, generation of precursor metabolites)[33] and other categories whose function in pathological LVH has not been previously defined (eg, regulation of RNA splicing, amino acid and derivative metabolism). This suggests that the differential wiring analysis can facilitate identification of novel molecular pathways in pathological LVH. For example, Paip2b-encoded (poly(A)-binding protein–interacting protein 2B) protein displaces poly(A)binding protein from the poly(A) tail of capped/polyadenylated mRNAs, thereby inhibiting translation.[34] Observed downregulation of Paip2b in pathological LVH samples is consistent with increased protein turnover in pathological LVH.[35] The cellular function of the *Tiprl* (TIP41, target of rapmycin signaling pathway regulator-like) gene has not been studied in the heart, but it was recently shown to inhibit mitogen activated protein kinase kinase7 -c-Jun N-terminal kinase activity in hepatocellular carcinoma through type 2A phosphatases.[36]

Consideration of gene rewiring may be a useful adjunct to traditional differential expression profiling approaches such as magnitude of fold change for several reasons. First, rewired genes are identified using data-driven analysis that, unlike differential expression profiling, does not depend on introduction of rigid significance thresholds. This is an important advantage given that predefined statistical thresholds may significantly alter microarray interpretation.[29] Second, because data sets are compared at the level of coexpression matrices, rewiring may be more sensitive to subtle expression changes, which are otherwise missed during conventional statistical comparison.

Finally, evaluation of rewiring patterns may uncover spatial relationships across gene neighborhoods, identifying higher-level biologically relevant pathways, thus presenting additional level of information within a microarray experiment.

Gene–Protein Relationships

An important issue is the magnitude of correlation between changes in mRNA and protein levels, which may reflect the relative importance of transcriptional regulation versus other mechanisms. To address this, we undertook a proteomics analysis focused on defined functional groups identified from the rewired gene network of pathological LVH. We analyzed the ECM and myofilament subproteome because functional gene groups encoding proteins involved in regulating these structures were identified as differentially rewired. The method used to enrich the extracellular and myofilament proteome also enriched mitochondrial proteins, which was another functional category identified as rewired. Although proteomics cannot provide a global analysis of all expressed cardiac proteins, focusing on a subproteome allowed us to identify 12 of 30 (40%), 80 of 226 (35%), and 22 of 102 (22%) rewired genes in myofilament, mitochondrial, and extracellular subproteomes. This finding confirms that enriching for specific subproteomes enhances the confidence of protein quantification.[37]

We found a modest positive correlation between changes in mRNA levels and protein abundance when assessing these at the individual gene level, especially for the specifically enriched subproteomes (myofilament and extracellular). This could be taken to indicate that nontranscriptional mechanisms, such as alterations in protein stability, are at least as important as transcriptional regulation. However, we found that mRNA–protein relationships analyzed at the Reactome pathway level were substantially stronger. This striking finding suggests that the expression of entire pathways may be controlled at the transcriptional level[38] and could, in part, be a manifestation of other mechanisms such as microRNA-mediated regulation.[39] In addition to validating the potential of network biology and differential wiring analyses to identify real biological changes in protein abundance, this finding also suggests that the network approach may identify pathways that may not be readily detected by conventional comparisons of microarray profiles. Pathways found to be correlated at the mRNA–protein level included several known to be involved in the regulation of LVH, such as upregulation of chondroitin sulfate metabolism[40] and the endothelial nitric oxide synthase pathway[41] and downregulation of S phase[42] and antigen processing-cross presentation[43] pathways.

Conclusions

Overall, our results represent a first attempt to provide insights into the integrated molecular mechanisms of pathological versus physiological cardiac hypertrophy by representing transcriptomic and proteomic data as biological networks. The methodology that we have developed is freely accessible at http://sites.google.com/site/cardionetworks. With the increasing availability of comprehensive omics data sets in the public domain, analytic approaches described herein may be useful for the elucidation of both general and specific mechanisms of cardiac diseases. Future expansion and modification of such methodology may be valuable in developing new therapeutic strategies or biomarkers.

Sources of Funding

This work was supported by the British Heart Foundation through awards RE/08/003 and CH//99001 (Dr Shah), a British Heart Foundation Senior Fellowship (Dr Mayr), and a PhD studentship (Dr Drozdov); a Leducq Fondation Transatlantic Network of Excellence; a National Institute for Health Research Biomedical Research Centre award to Guy's & St Thomas' National Health Service (NHS) Trust with King's College London and King's College Hospital NHS Trust; and a European Commission Network of Excellence ENFIN (contract number LSHG-CT-2005-518254) to Dr Ouzounis.

Disclosures

Dr Drozdov is a managing director at Bering Ltd. The company had no role in design, analysis, or funding of this work. The other authors report no conflicts.

References

1. Heineke J, Molkentin JD. Regulation of cardiac hypertrophy by intracellular signalling pathways. *Nat Rev Mol Cell Biol*. 2006;7:589–600.
2. Towbin JA, Bowles NE. The failing heart. *Nature*. 2002;415:227–233.
3. Catalucci D, Latronico MV, Ellingsen O, Condorelli G. Physiological myocardial hypertrophy: how and why? *Front Biosci*. 2008;13:312–324.
4. Shah AM, Mann DL. In search of new therapeutic targets and strategies for heart failure: recent advances in basic science. *Lancet*. 2011;378:704–712.
5. Bandyopadhyay S, Mehta M, Kuo D, Sung MK, Chuang R, Jaehnig EJ, et al. Rewiring of genetic networks in response to DNA damage. *Science*. 2010;330:1385–1389.
6. Lusis AJ, Weiss JN. Cardiovascular networks: systems-based approaches to cardiovascular disease. *Circulation*. 2010;121:157–170.
7. Pujana MA, Han JD, Starita LM, Stevens KN, Tewari M, Ahn JS, et al. Network modeling links breast cancer susceptibility and centrosome dysfunction. *Nat Genet*. 2007;39:1338–1349.
8. Dewey FE, Perez MV, Wheeler MT, Watt C, Spin J, Langfelder P, et al. Gene coexpression network topology of cardiac development, hypertrophy, and failure. *Circ Cardiovasc Genet*. 2011;4:26–35.
9. Zhu W, Yang L, Du Z. Layered functional network analysis of gene expression in human heart failure. *PLoS One*. 2009;4:e6288.
10. Rajan S, Williams SS, Jagatheesan G, Ahmed RP, Fuller-Bicer G, Schwartz A, et al. Microarray analysis of gene expression during early stages of mild and severe cardiac hypertrophy. *Physiol Genomics*. 2006;27:309–317.
11. Bernardo BC, Weeks KL, Pretorius L, McMullen JR. Molecular distinction between physiological and pathological cardiac hypertrophy: experimental findings and therapeutic strategies. *Pharmacol Ther*. 2010;128:191–227.
12. Parkinson H, Kapushesky M, Kolesnikov N, Rustici G, Shojatalab M, Abeygunawardena N, et al. ArrayExpress update–from an archive of functional genomics experiments to the atlas of gene expression. *Nucleic Acids Res*. 2009;37(Database issue):D868–D872.
13. Watson-Haigh NS, Kadarmideen HN, Reverter A. PCIT: an R package for weighted gene co-expression networks based on partial correlation and information theory approaches. *Bioinformatics*. 2010;26:411–413.
14. Jeong H, Mason SP, Barabási AL, Oltvai ZN. Lethality and centrality in protein networks. *Nature*. 2001;411:41–42.
15. Feldman I, Rzhetsky A, Vitkup D. Network properties of genes harboring inherited disease mutations. *Proc Natl Acad Sci U S A*. 2008;105:4323–4328.
16. Fuller TF, Ghazalpour A, Aten JE, Drake TA, Lusis AJ, Horvath S. Weighted gene coexpression network analysis strategies applied to mouse weight. *Mamm Genome*. 2007;18:463–472.
17. Byrne JA, Grieve DJ, Bendall JK, Li JM, Gove C, Lambeth JD, et al. Contrasting roles of NADPH oxidase isoforms in pressure-overload versus angiotensin II-induced cardiac hypertrophy. *Circ Res*. 2003;93:802–805.
18. De Bono JP, Adlam D, Paterson DJ, Channon KM. Novel quantitative phenotypes of exercise training in mouse models. *Am J Physiol Regul Integr Comp Physiol*. 2006;290:R926–R934.
19. Barallobre-Barreiro J, Didangelos A, Schoendube FA, Drozdov I, Yin X, Fernández-Caggiano M, et al. Proteomics analysis of cardiac extracellular

matrix remodeling in a porcine model of ischemia/reperfusion injury. *Circulation*. 2012;125:789–802.
20. Yin X, Cuello F, Mayr U, Hao Z, Hornshaw M, Ehler E, et al. Proteomics analysis of the cardiac myofilament subproteome reveals dynamic alterations in phosphatase subunit distribution. *Mol Cell Proteomics*. 2010;9:497–509.
21. Smyth GK. Limma: linear models for microarray data. In: Gentleman R, Carey V, Dudoit S, Irizarry R, Huber W, ed. *Bioinformatics and Computational Biology Solutions Using r and Bioconductor*. New York: Springer; 2005:397–420.
22. Weng MP, Liao BY. MamPhEA: a web tool for mammalian phenotype enrichment analysis. *Bioinformatics*. 2010;26:2212–2213.
23. Clauset A, Newman ME, Moore C. Finding community structure in very large networks. *Phys Rev E Stat Nonlin Soft Matter Phys*. 2004;70(6 pt 2):066111.
24. Nabieva E, Jim K, Agarwal A, Chazelle B, Singh M. Whole-proteome prediction of protein function via graph-theoretic analysis of interaction maps. *Bioinformatics*. 2005;21(suppl 1):i302–i310.
25. Albert R, Jeong H, Barabasi AL. Error and attack tolerance of complex networks. *Nature*. 2000;406:378–382.
26. Zelezniak A, Pers TH, Soares S, Patti ME, Patil KR. Metabolic network topology reveals transcriptional regulatory signatures of type 2 diabetes. *PLoS Comput Biol*. 2010;6:e1000729.
27. Matthews L, Gopinath G, Gillespie M, Caudy M, Croft D, de Bono B, et al. Reactome knowledge base of human biological pathways and processes. *Nucleic Acids Res*. 2009;37(Database issue):D619–D622.
28. Kong SW, Bodyak N, Yue P, Liu Z, Brown J, Izumo S, et al. Genetic expression profiles during physiological and pathological cardiac hypertrophy and heart failure in rats. *Physiol Genomics*. 2005;21:34–42.
29. Dalman MR, Deeter A, Nimishakavi G, Duan ZH. Fold change and p-value cutoffs significantly alter microarray interpretations. *BMC Bioinformatics*. 2012;13(suppl 2):S11.
30. Aggarwal A, Guo DL, Hoshida Y, Yuen ST, Chu KM, So S, et al. Topological and functional discovery in a gene coexpression meta-network of gastric cancer. *Cancer Res*. 2006;66:232–241.
31. Mandl A, Huong Pham L, Toth K, Zambetti G, Erhardt P. Puma deletion delays cardiac dysfunction in murine heart failure models through attenuation of apoptosis. *Circulation*. 2011;124:31–39.
32. Drozdov I, Tsoka S, Ouzounis CA, Shah AM. Genome-wide expression patterns in physiological cardiac hypertrophy. *BMC Genomics*. 2010;11:557.
33. McCurdy S, Baicu CF, Heymans S, Bradshaw AD. Cardiac extracellular matrix remodeling: fibrillar collagens and Secreted Protein Acidic and Rich in Cysteine (SPARC). *J Mol Cell Cardiol*. 2010;48:544–549.
34. Berlanga JJ, Baass A, Sonenberg N. Regulation of poly(A) binding protein function in translation: characterization of the Paip2 homolog, Paip2B. *RNA*. 2006;12:1556–1568.
35. Proud CG. Ras, PI3-kinase and mTOR signaling in cardiac hypertrophy. *Cardiovasc Res*. 2004;63:403–413.
36. Song IS, Jun SY, Na HJ, Kim HT, Jung SY, Ha GH, et al. Inhibition of MKK7-JNK by the TOR signaling pathway regulator-like protein contributes to resistance of HCC cells to TRAIL-induced apoptosis. *Gastroenterology*. 2012;143:1341–1351.
37. Didangelos A, Yin X, Mandal K, Baumert M, Jahangiri M, Mayr M. Proteomics characterization of extracellular space components in the human aorta. *Mol Cell Proteomics*. 2010;9:2048–2062.
38. Washburn MP, Koller A, Oshiro G, Ulaszek RR, Plouffe D, Deciu C, et al. Protein pathway and complex clustering of correlated mRNA and protein expression analyses in Saccharomyces cerevisiae. *Proc Natl Acad Sci U S A*. 2003;100:3107–3112.
39. Da Costa Martins PA, De Windt LJ. MicroRNAs in control of cardiac hypertrophy. *Cardiovasc Res*. 2012;93:563–572.
40. Ridinger H, Rutenberg C, Lutz D, Buness A, Petersen I, Amann K, et al. Expression and tissue localization of beta-catenin, alpha-actinin and chondroitin sulfate proteoglycan 6 is modulated during rat and human left ventricular hypertrophy. *Exp Mol Pathol*. 2009;86:23–31.
41. Carnicer R, Crabtree MJ, Sivakumaran V, Casadei B, Kass DA. Nitric oxide synthases in heart failure. *Antioxid Redox Signal*. 2013;18:1078–1099.
42. Ahuja P, Sdek P, MacLellan WR. Cardiac myocyte cell cycle control in development, disease, and regeneration. *Physiol Rev*. 2007;87:521–544.
43. Galindo CL, Skinner MA, Errami M, Olson LD, Watson DA, Li J, et al. Transcriptional profile of isoproterenol-induced cardiomyopathy and comparison to exercise-induced cardiac hypertrophy and human cardiac failure. *BMC Physiol*. 2009;9:23.

CLINICAL PERSPECTIVE

A fundamental question in heart failure research is to understand why disease stresses, such as hypertension, lead to pathological cardiac hypertrophy and an accompanying risk of heart failure whereas physiological stresses, such as exercise or pregnancy, lead to physiological cardiac remodeling without major risk of heart failure. Previous studies have investigated the roles of specific molecular signaling pathways or have analyzed differences in gene expression in experimental models to try and identify similarities and differences between physiological and pathological hypertrophy. In the current work, a global network biology approach was developed using genomic and proteomic data from multiple experimental mouse models to study the molecular patterns that distinguish pathological and physiological hypertrophy. A network-based combined analysis of 127 publicly available genome-wide expression arrays using graph theory methods was able to define phenotype-specific pathological and physiological gene coexpression networks. A key difference in network structure between the physiological and pathological networks was rewiring of a subset of genes, that is, their differential coexpression in the 2 networks. This rewired network included several distinct cellular pathways and gene sets. Furthermore, targeted proteomic analysis revealed significant mRNA–protein correlation at the cellular pathway level (eg, for extracellular matrix components). This combined gene network and proteomic analysis of left ventricular hypertrophy provides a platform for the identification and investigation of potentially novel pathways that distinguish physiological and pathological hypertrophy. In addition, a detailed freely accessible protocol is provided that allows similar analyses in other cardiovascular diseases.

SUPPLEMENTAL MATERIAL

Materials and Methods

Microarray acquisition, pre-processing, and quality control

Six mouse microarray datasets (n = 127 arrays) were obtained from the ArrayExpress database[1] (**Table 1**). The datasets that were chosen for study represented different surgical/exercise and genetic models of pathological or physiological hypertrophy based on the respective phenotypes. The pathological cohort comprised a cardiomyocyte-specific AT1 (angiotensin receptor type 1) transgenic heart dataset and two surgical AC (aortic constriction) datasets. The AT1 dataset consisted of wild type mice (n = 5), and the AT1 transgenics undergoing cardiac failure and hypertrophy (n = 11). The AC1 dataset included time course data for untreated (n = 3), sham (n = 6), and AC (n = 10) operated male mice. The AC2 dataset consisted of time course data monitoring mice undergoing aortic constriction (n = 18) and sham- (n = 18) operated controls. The physiological cohorts included Akt, PI3K, and Swimming datasets. The Akt dataset consisted of normal heart tissue (n = 4), short-term (2 weeks) activated cardiac-specific Akt1 overexpression (n = 4), and switched-off Akt1 (2 days following 2 week activation, n = 4). The PI3K dataset consisted of wild type hearts (n = 3) and cardiac-specific overexpression of dominant-negative PI3K (n = 3) or a constitutively active form of PI3K (n = 3). Finally, the Swimming dataset, containing 30 arrays, monitored expression in mouse hearts under normal conditions, swimming (short- and long-term), and swimming followed by 1 week of rest. Mice were swum for 10 min – 90min twice a day. Mice were sacrificed at 10 min, 2.5 days, one week, two weeks, three weeks, or 4 weeks of exercise training, and after 4 weeks of swimming and one week of rest. Age-matched mice that did not exercise were used as controls. Heart weight/body weight ratios were increased with exercise by 29-49% ($p<0.05$). Detailed morphological and experimental data on this model can be obtained from http://cardiogenomics.med.harvard.edu/groups/proj1/pages/swim_home.html.Where applicable, raw expression values were normalized using Robust Multi-array Average (RMA)[2] pipeline available through the affy[3] package for R statistical environment. If raw array data was not readily available, processed gene expression profiles were log2-transformed. To standardize multiple microarray platforms, Affymetrix probe names were mapped to Entrez gene identifiers (IDs)[4] and in cases where multiple probesets mapped to a single gene, the probeset with largest inter-array variance in signal intensity was retained.

We then calculated the correlation of gene expression between samples, and outliers with mean sample correlations more than three standard deviations below average were omitted until no outliers remained[5]. After outlier detection, quantile normalization was performed on the filtered data.

Reverse engineering gene networks and generation of random networks

Gene co-expression networks

Pairwise similarity in gene expression vectors was expressed by the Pearson correlation coefficient (PCC). Gene pairs that correlated above a predefined PCC threshold were represented in the form of an undirected unweighted network, where nodes correspond to genes and links (edges) correspond to co-expression between genes. We used the partial correlation and information theory (PCIT) algorithm to eliminate non-significant co-expressions for each microarray dataset[6]. This algorithm uses first-order partial correlation coefficients combined with an information theory approach to identify meaningful gene–gene associations. Briefly, the strength of the linear correlation is assessed between two genes

given its independence from a third gene. It has previously been applied to reverse-engineered gene co-expression networks in human B cells[7] and elucidation of metabolic pathways in Saccharomyces cerevisiae[8].

Random network generation

To compare real gene co-expression networks to randomly generated networks, we computed 200 random networks using the Maslov-Sneppen approach[9]. Randomization was performed by rewiring edges in the original networks while preserving degrees of the respective nodes. The number of rewiring steps taken for each model was 4 x (number of edges).

Graph theory methods

Node degree

The most elementary characteristic of a node is its degree, k, which indicates how many links the node has to other nodes. Degree is associated with the importance of a node, or its centrality with respect to other nodes in the network. Node degree of the i^{th} gene is defined by

$$k = \sum_{j \neq i} A(i,j)$$

where **A** is the symmetric adjacency matrix of a gene network. In biological networks, such as the yeast protein interaction network, nodes with high degree, also known as hubs, appear to be essential for cell survival[10].

Betweenness centrality

Betweenness centrality (C^{Btw}) can help to identify nodes with high information flow. Betwenness centrality of a node *i* in an unweighted and undirected network is given by:

$$C^{Btw(i)} = \sum_{j<k} \frac{g_{jk}(i)}{g_{jk}}$$

where $g_{jk}(i)$ is the number of shortest paths between nodes *j* and *k* that pass through node *i* and g_{jk} is the total number of shortest paths connecting nodes *j* and *k*. Therefore, nodes with the highest betweenness control most of the information flow in the network, representing the critical points of the network. In yeast regulatory networks, these nodes appear to have a higher tendency to be essential genes[11].

Eigenvector centrality

Eigenvector centrality (C^{Eig}) favors nodes that are connected to nodes that are themselves central within the network, thus taking into account overall network connectivity[12]. The C^{Eig} of a node *i* in an unweighted and undirected network is given by:

$$C^{Eig(i)} = \frac{1}{\lambda} \sum_{j \in M(i)} x_j = \frac{1}{\lambda} \sum_{j=1}^{N} A_{i,j} x_j$$

where **A** is the adjacency matrix, *N* is number of nodes, *M(i)* is a set of neighbor nodes of *i*, and λ is the largest eigenvalue. For example, in protein-protein interaction networks, C^{Eig} is a measure for how well connected a protein is to other highly connected proteins in a network.

Clustering coefficient

Clustering coefficient, C^{Clu}, intends to answer the question: in what percentage of cases, a node's neighbors are also neighbors. For node *i*, $C^{Clu(i)}$ is defined as:

$$C^{Clu(i)} = \frac{2n}{k_i(k_i - 1)}$$

where *n* denotes the number of direct links connecting the k_i nearest neighbors of node *i*. C^{Clu} ranges from zero (for a node that is part of a loosely connected group) to one (for a node at the center of a fully connected cluster). Thus, C^{Clu} measures the local clustering in the graph. In protein-protein interaction networks, genes that harbor a disease-causing mutation tend to avoid dense-clustering neighborhoods, unlike the genes that are essential for cell survival[13].

Density

The density of a graph is defined as the ratio of the number of edges to the number of possible edges. Density values range between 0 and 1. In the former case, a graph is disconnected, while in the latter case, every vertex of the graph is fully interconnected.

Shortest path

The shortest path for an undirected and unweighted graph is defined as the shortest sequence of steps (i.e. distance) to be travelled between any two genes in a network. A graph theoretic analysis of metabolic reactions in Escherichia coli has revealed a larger than expected shortest path length (~8 reactions), suggesting that the metabolic world of this organism is not small in terms of biosynthesis and degradation[14].

Diameter

Diameter is defined as the longest shortest path between any two nodes in a network. In an unweighted and undirected graph, it is the highest number of hops to be traveled between any two nodes. Interestingly, most real networks have surprisingly small diameters, and thus they can be classified as "small-world". The idea comes from Stanley Milgram's experiment in 1969[15], who found that the average distance that letters have to travel in a social network (which was not visible a priori) was 6, hence the phrase "six degrees of separation".

K-core decomposition

The *k*-core of a graph is defined as the maximum subgraph if every node has at least *k* links. *K*-core is determined by iteratively pruning all nodes with a degree lower than *k* and their incident links. The cores of a graph form layers: the (*k*+1)-core is always a subgraph of the *k*-core. Consequently, a subgraph with higher coreness will contain nodes with higher degrees. Application of a core decomposition method recently allowed identification of the inherent layer structure of the yeast protein interaction network, whereby probability of proteins both being essential and evolutionary conserved successively increased toward the innermost cores[16].

Gene community detection

In Pathological and Physiological networks gene communities were identified by optimization of modularity[17, 18]. The method is a greedy optimization procedure that attempts to optimize the modularity of a partition of the network. Modularity, *Q*, is defined as the fraction of all edges that lie within communities minus the expected value of the same quantity in a graph in which the vertices have the same degrees but edges are placed randomly[18]. It is given by:

$$Q = \sum_{s=1}^{NC} \frac{E_s}{E} - \left(\frac{k_s}{2E}\right)^2$$

Where, *NC* is the number of clusters, *E* is the number of edges in the network, E_s is the number of edges between vertices within cluster *s*, and k_s is the sum of the degrees of the vertices in cluster *s*. The value of the modularity measure *Q* ranges from 0 to 1, and the optimal clustering is achieved by maximizing *Q*.

Graph-theoretic analyses were carried out using the Functional Genomic Assistant toolbox[19] for MATLAB (2009a, The MathWorks, Nattick MA) and the *igraph*[20] library for R statistical environment.

Phenotype and gene set enrichment analyses

To determine phenotype-specificity of the Pathological and Physiological networks, we used the MamPhEA web tool[21] for mammalian phenotype enrichment analysis. Phenotype information was acquired from the MGI database[22]. Individual gene sets were enriched for Gene Ontlogy (GO) Biological Process (BP) and Cellular Component (CC) terms. Additionally, pathway level enrichment was performed using the Reactome pathway database[23]. Enrichment analysis was performed using the model-based gene set enrichment analysis (MGSA)[24]. MGSA employs probabilistic inference via a Metropolis-Hasting algorithm to estimate the probability of categories to be active. The MGSA approach naturally takes category overlap into account and avoids the need for multiple testing corrections met in single-category enrichment analysis. All relevant gene sets were acquired from the Molecular Signatures Database (MSigDB, v3.0)[25].

Animal models

Procedures were performed in accordance with the Guidance on the Operation of the Animals (Scientific Procedures) Act, 1986 (United Kingdom). Pathological cardiac hypertrophy was induced by the minimally invasive aortic constriction (AC), as previously described[26]. C57BL/6 mice 8-10 weeks of age were used. Sham constriction involved identical surgery apart from band placement. Physiological cardiac hypertrophy was achieved by a voluntary wheel running program[27]. Briefly, 8-10 weeks old C57BL/6 mice were initially introduced together into the running cage to learn from each other to run on the wheel. After a 7 day training period, mice were randomly housed individually and left to run up to 4 weeks. The running wheel is connected by a light triggered counting system, running time and distance is monitored and recorded with LabChart7. The average running distance was over 4km/day. Age-matched mice were also randomly assigned to the sedentary control group. They were housed in identical cages except for a non-rotating wheel for the same amount of time. 2 weeks TAC and 4 weeks exercise running resulted in 65% and 14% increase compared to controls in terms of heart weight/tibia length ratio respectively (**Supplementary Figure S4**).

qPCR assay

RNA was extracted from mouse tissue using the RNeasy Mini Kit (Qiagen) according to the manufacturer's protocol. 1 µg of total RNA was reverse transcribed into cDNA with the High Capacity RNA to cDNA kit (Life tech). The reverse transcription (RT) was performed according to the company's recommendations (10 µl of 2x Reverse-Transcription Buffer combined with 1 µl of 20x Reverse Transcription Enzyme mix) to a final volume of 20 µl. The RT reaction was set as follows: 37°C for 60 min and 95°C for 5 min using a Veriti thermocycler (Applied Biosystems). Taqman gene expression assays were used to assess the expression of individual genes: Col1a1, Col4a1, Col5a2, Paip2b, Phtf2, Prps1, Rnf14, Serpinh1, Sparc, Tiprl (Life Tech). For each gene, 10 ng of cDNA were combined with 0.5 µl

of Taqman gene expression Assay (20x) (Applied Biosystems) and 5 µl of the Taqman Universal PCR Master Mix No AmpErase UNG (2x) to a final volume of 10 µl. Quantitative PCR was performed on an Applied Biosystems 7900HT thermocycler at 95°C for 10 min, followed by 40 cycles of 95°C for 15 sec and 60°C for 1 min. All samples were standardized to Gapdh using SDS2.2 (Applied Biosystems) software.

Animal models for proteomic experiments

The *in vivo* models of pathological hypertrophy that were studied have been described previously[28]. Wild-type mice (n = 4) underwent implantation of osmotic minipumps, and received angiotensin II (1.1mg/kg/day) for 14 days. Pressure overload was induced by aortic constriction in wild-type mice (n = 4) anesthetized with an isoflurane/O_2 mixture (2/98%). Sham surgery (n = 4) comprised an identical procedure with the exception of constriction. Tissues were obtained at 2 weeks post-surgery.

Tissue preparation

For the proteomics studies, we used LVs from 4 wild-type sham-operated mice, 3 angiotensin II-induced hypertrophy and 3 LVs following aortic constriction. Protein extraction was performed as described previously[29]. In brief, to remove plasma contaminants LVs were diced into small pieces and incubated with 0.5M NaCl, 10mM Tris pH 7.5, plus proteinase/phosphatase inhibitor cocktails (Sigma-Aldrich) and 25mM EDTA. To partially decellularize the hearts and skin the cardiomyocytes, samples were incubated with 0.1% SDS (10:1 buffer volume to tissue weight), including proteinase/phosphatase inhibitor cocktails and 25mM EDTA. Finally, to solubilize heavily crosslinked extracellular matrix (ECM) and myofilament proteins, samples were incubated in a 4M guanidine-HCl, 50mM sodium acetate pH 5.8 buffer (5:1 buffer volume to tissue weight), plus proteinase/phosphatase inhibitor cocktails and 25mM EDTA. Subsequently, deglycosylation (removal of glycosaminoglycan side chains) was achieved by enzymes (0.05U, chondroitinase ABC [*Proteus vulgaris*], keratanase [*Bacteroides fragillis*], heparatinase II [*Flavobacterium heparinum*], Sygma Aldrich) in a 150mM NaCl, 50mM sodium acetate pH 6.8 buffer supplemented with proteinase/phosphatase inhibitors and 10mM EDTA for 16h at 37^{o}C.

1D Electrophoresis

Aliquots of the guanidine extracts were denatured and reduced in sample buffer containing 100mM Tris, pH 6.8, 40% glycerol, 0.2% SDS, 2% beta-mercaptoethanol and 0.02% bromophenol blue and boiled at 96^{0}C for 10min. 35µg of protein per sample were loaded and separated on Bis-Tris discontinuous 4-12% polyacrylamide gradient gels (NuPage, Invitrogen). Pre-stained protein standards were run alongside the samples to allow molecular mass estimation of proteins (All Blue, Precision Plus, Bio-Rad Laboratories).

Nanoflow liquid chromatography tandem mass spectrometry (LC-MS/MS)

After electrophoresis, Coomassie staining was used for band excision to avoid cross-contamination of fainter gel bands. To ensure equal loading in each LC-MS/MS experiment, the entire gel lane was excised and subjected to in-gel digestion with trypsin using an Investigator ProGest (Genomic Solutions) robotic digestion system. Tryptic peptides were separated on a nanoflow LC system and eluted with an 80 min gradient (10-25% B in 35 min, 25-40% B in 5 min, 90% B in 10 min and 2% B in 30min where A=2% ACN, 0.1% formic acid in HPLC H_2O and B = 90% ACN, 0.1% formic acid in HPLC H_2O). The column was coupled to a nanospray source (Picoview). After the direct LC-MS run, the flow was switched and the portion stored in the capillary of the RePlay (Advion) device reanalyzed ('replay run'). This injection system splits the gradient from the analytical column and allows the re-analysis of the same sample in a single LC-MS/MS run[30]. Spectra were collected from an ion-trap mass analyzer (LTQ Orbitrap XL, ThermoFisher Scientific) using full ion scan mode over the mass-to-charge (m/z) range 450-1600. MS/MS was performed on the top six ions in each MS scan using the data-dependent acquisition mode with dynamic exclusion enabled.

MS/MS peaklists were generated by extract_msn.exe and matched to mouse database (UniProtKB/Swiss-Prot) using SEQUEST v.28 (rev. 13), (Bioworks Browser 3.3.1 SP1, ThermoFisher Scientific) and X! Tandem, (Version 2007.01.01.2). Carboxyamidomethylation of cysteine was chosen as fixed modification and oxidation of methionine as variable modification. The mass tolerance was set at 1.5 AMU for the precursor ions and at 1.0 AMU for fragment ions. Two missed cleavages were allowed.

Label-free quantification

Spectral counts

Scaffold (version 2.0.6, Proteome Software Inc., Portland, OR) was used to calculate the spectral counts and to validate MS/MS based peptide and protein identifications[31, 32]. According to the default values in the Scaffold software, the following peptide thresholds were applied: X! Tandem: -Log(Expect Scores) > 2.0, SEQUEST: deltaCn > 0.10 and XCorr > 2.5 (+2), 3.5 (+3) and 3.5 (+4). Peptide identifications were accepted if they could be established at greater than 95.0% probability as specified by the Peptide Prophet algorithm [31]. Protein identifications were accepted if they could be established at greater than 99.0% probability with at least 2 independent peptides. RePlay samples were combined using the Scaffold software. Spectral counts were $\log_2$-transformed in order to increase the signal of low-abundant proteins.

Ion intensity

Progenesis LC-MS software (Version 3.1; Nonlinear Dynamics Ltd., Newcastle, UK) was used to perform protein relative quantification based on peptide ion abundance. To analyse the data from fractionated samples, a series of experiments was created with the software. An "experiment" was created by combining the LC-MS/MS runs of analogous fractions from each biological sample. The raw data containing LC-MS analyses acquired in profile mode with a high resolution mass spectrometer were uploaded, and for each experiment, the most representative LC-MS run was selected as reference run. The LC-MS patterns were then aligned with the reference run setting alignment vectors automatically to compensate for between-run variation in the LC separation technique. After inspection of the alignment results, additional vectors were manually inserted where needed. Peptide peaks were automatically detected and filtered based on charge state (only +2, +3 and +4 charges were selected). Subsequently, +4 charged peptides with 2 or less isotopes were removed from the analysis. The peptide ion abundance was then calculated as the sum of the peak areas within the isotopes boundaries. To correct experimental/technical variations, the peptide ion abundance was automatically normalized by calculation of a robust distribution of all peptide abundance ratios and determination of a global scaling factor. Peptide and protein identification was obtained from the Scaffold spectrum report containing the MS/MS search results. The protein abundance was then calculated as the sum of the abundances of all unique peptides belonging to the protein. Proteins were collated by combination of the single-fraction experiments in one overall multi-fraction experiment. Relative protein quantification between groups (*e.g.* treated vs. control) was considered for proteins having two or more unique quantified peptides. RePlay samples were treated as technical replicates and raw protein intensity values were $\log_2$-transformed prior to further statistical analysis.

A comparison of protein spectral counting (SpC) and ion intensity (IoI) quantification is shown in **Supplementary Figure S6**, and indicates a significant correlation between the two approaches.

Proteomic data availability

Spectral counting and ion intensity reports are available in **Datasets 1 and 2** respectively.

Western blotting

Aliquots of the SDS and 4M guanidine extracts were mixed with denaturing sample buffer and boiled. 30μg of protein per sample were loaded and separated on 4-12% gradient gels as above. Proteins were then transferred on nitrocellulose membranes. Membranes were blocked in 5% fat-free milk powder in PBS and probed for 16h at 4ºC with primary antibodies to: TNNI3 (Abcam, ab10231), COL6A2 (Santa Cruz, sc-9855), GPX3 (RND Systems, AF4199), ITA8 (Santa Cruz, sc-25713) and β-Actin (Sigma-Aldrich, A5691). All antibodies were used at 1:500 dilution in 5% BSA. The membranes were treated with the appropriate secondary, horseradish peroxidase (HRP) conjugated antibodies (Dako) at a 1:2000 dilution. Finally, the blots were imaged using enhanced chemilluminenscence (ECL, GE Healthcare) and films were developed on a Xograph processor.

Statistical analysis

Differential expression analysis was performed by fitting a linear model with Empirical Bayes shrinkage to the log-intensities of expression values for each gene[33]. P-values were adjusted to control the expected false discovery rate using Benjamini-Hochberg correction. Adjusted p-values<0.05 were considered significant.

Analysis of protein functional categories

Functional enrichment analysis of proteins for Gene Ontology (GO) Cellular Process was performed using Enrichment Map tool[34].

Supplementary Figures

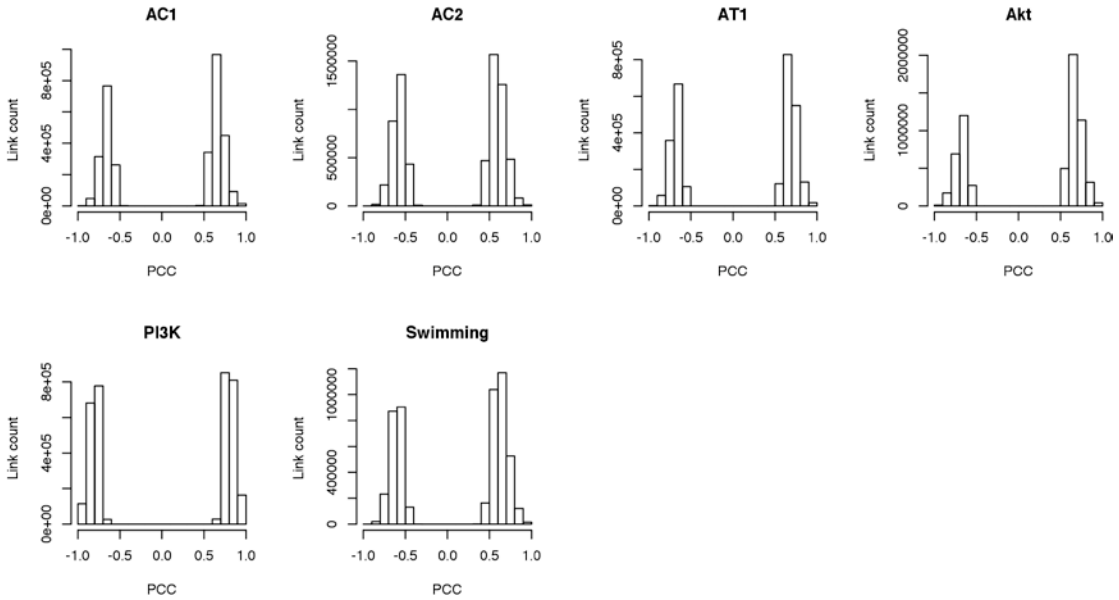

Supplementary Figure S1. Histograms visualizing distribution of positive and negative Pearson Correlation Coefficients (PCCs) for all mouse microarray datasets. The PCIT algorithm[6] was used to identify meaningful gene-gene co-expressions. All PCC values appear to be centered around ±0.75, suggesting a reasonable distribution of all coefficients.

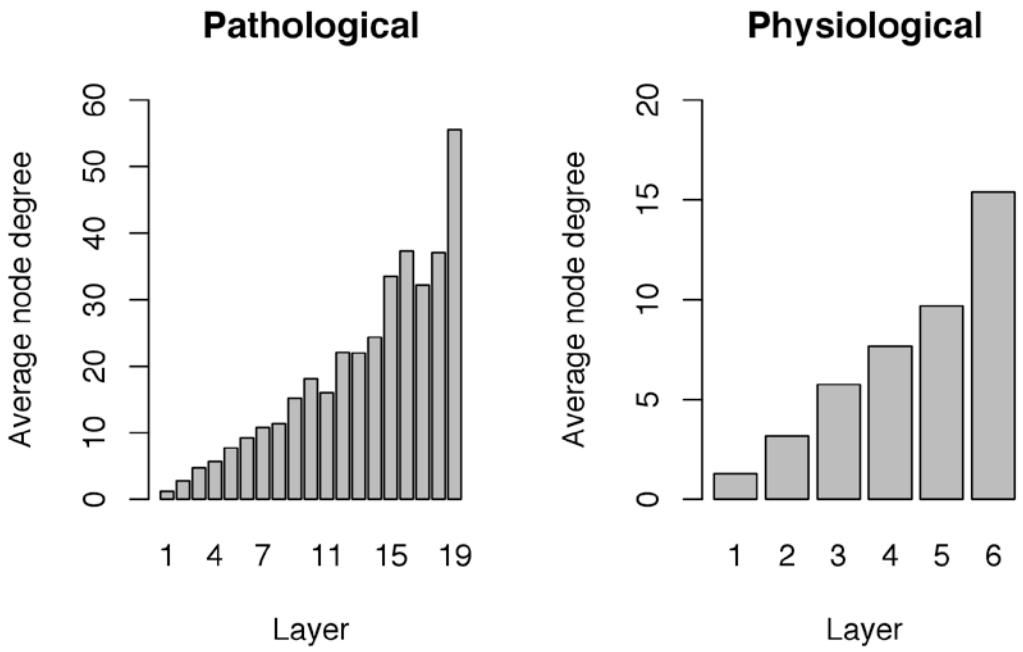

Supplementary Figure S2. Histograms demonstrating average node degrees of network layers in Pathological and Physiological networks.

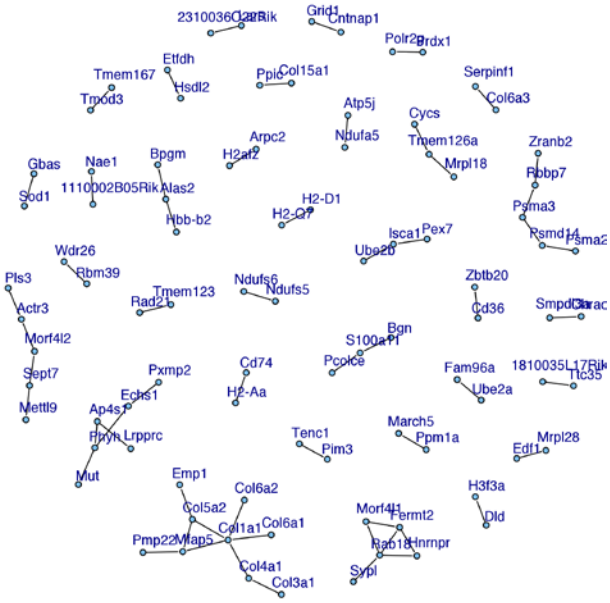

Supplementary Figure S3. Conserved nodes (n=90) and co-expressions (n=60) in both Pathological and Physiological networks. Each node and edge represents a gene and a co-expression that was observed in both LVH networks. Most of the shared co-expressions were between genes encoding extracellular matrix (ECM) proteins, for instance collagens (Col1a1, Col4a1, Col5a2, Col6a2) and serpin peptidase inhibitor clade F member 1 (Serpinf1).

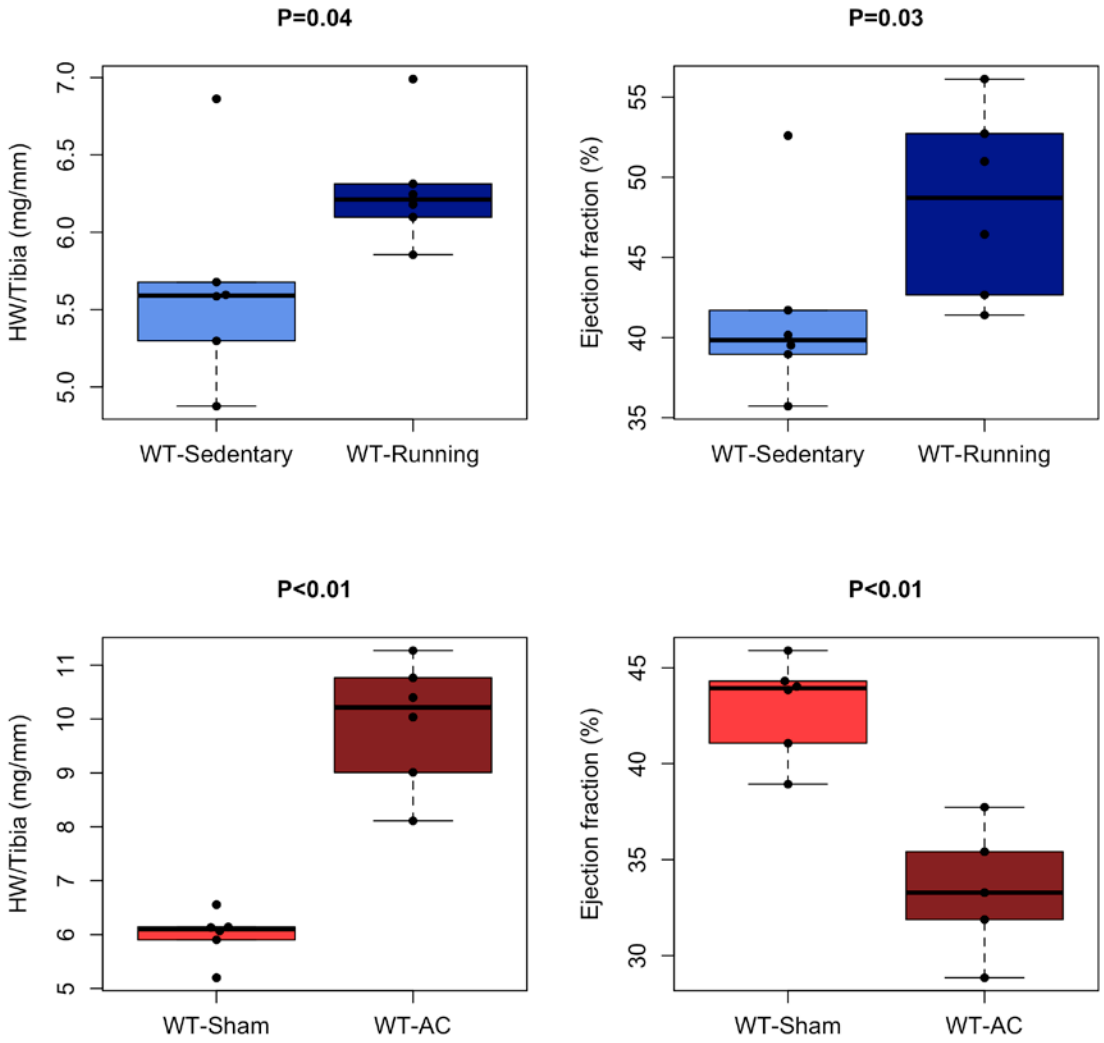

Supplementary Figure S4A. Morphological data for AC and exercised-trained mice and corresponding WT controls. Student t-test p-values < 0.05 were considered statistically significant. LV = left ventricle, HW = heart weight.

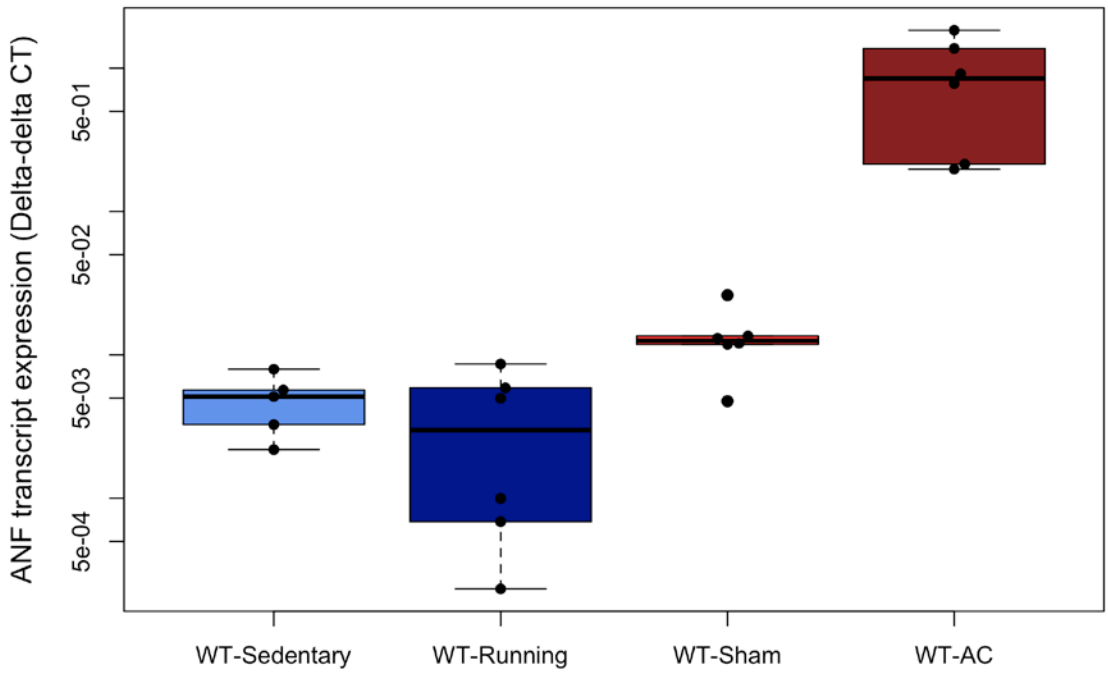

Supplementary Figure S4B. Atrial natriuretic peptide (ANF) transcript expression profiles in AC and exercised-trained mice and corresponding WT controls.

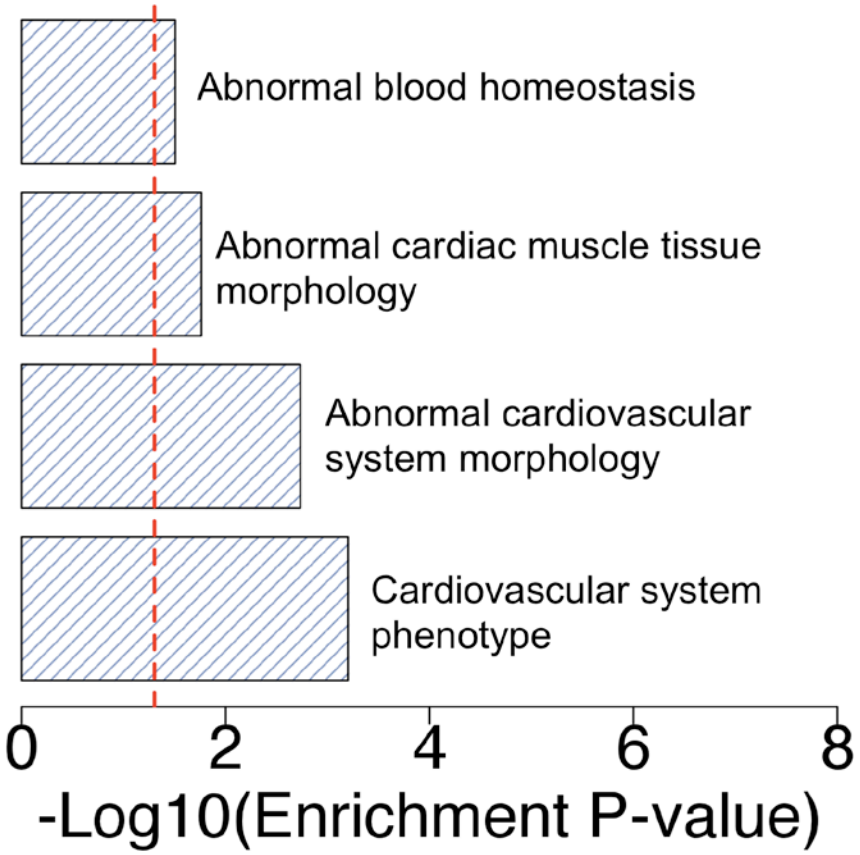

Supplementary Figure S5. MamPhEA-driven enrichment of genes common to the Pathological and Physiological networks for phenotypes associated with mutations in these genes. Dotted red line corresponds to adjusted p-value = 0.05.

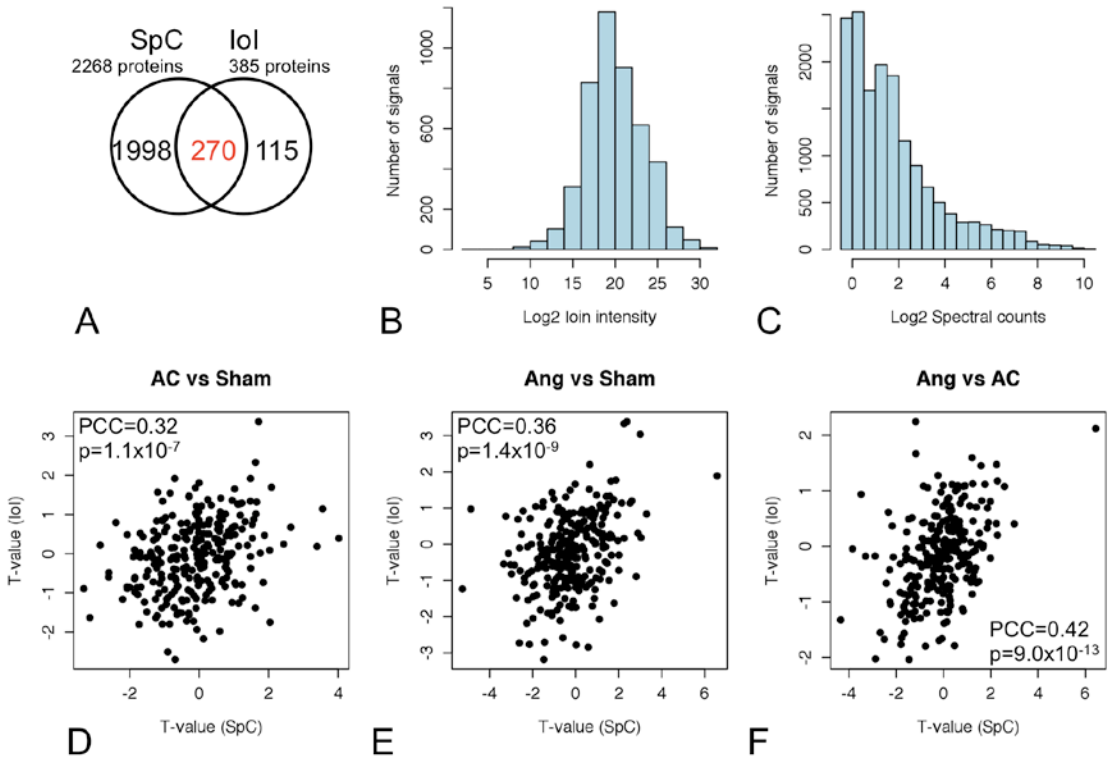

Supplementary Figure S6. **Comparison of protein spectral counting (SpC) with ion intensity (IoI) quantification. A)** Venn diagram showing 270 proteins identified by both quantification methods. **B)** Frequency histogram showing distribution of spectral counts across 2268 proteins. **C)** Frequency histogram showing distribution of spectral counts across 385 proteins. **D-F)** Pair-wise scatter plots between aortic constriction- (AC), angiotensin- (Ang), and sham-operated mice showing protein expression changes computed using either spectral counting or ion intensity quantification. Overall, there exists a significantly positive Pearson's correlation (PCC) between the two quantification approaches.

Supplementary Data

The following source data are available at: https://sites.google.com/site/cardionetworks/

Supplementary Table 1. Pathological LVH Network (3634 nodes, 13558 edges). Provided as Drozdov_TableS1.xls

Supplementary Table 2. Physiological LVH Network (3156 nodes, 4486 edges). Provided as Drozdov_TableS2.xls

Supplementary Table 3. Annotation and topology of 3634 genes in the Pathological network sorted by node degree. Provided as Drozdov_TableS3.xls

Supplementary Table 4. Annotation and topology of 3156 genes in the Physiological network sorted by node degree. Provided as Drozdov_TableS4.xls

Supplementary Table 7. Annotation and topology of 1553 genes in the Rewired network sorted by the degree of rewiring. Provided as Drozdov_TableS7.xls

Supplementary Table 9. Pathological hypertrophy mitochondrial, myofilament, and extracellular subproteomes. Provided as Drozdov_TableS9.xls

Supplementary Table 10. Differential expression information for assigned protein spectra and corresponding gene expression in pathological hypertrophy datasets. Provided as Drozdov_TableS10.xls

Supplementary Table 11. Average mRNA and protein fold changes for respective Reactome pathways. Table is sorted by decreasing mRNA level fold change. Provided as Drozdov_TableS11.xls

Supplementary Dataset 1. Protein spectra counts in cardiac hypertrophy. Provided as Drozdov_Dataset1.xls

Supplementary Dataset 2. Protein ion intensities in cardiac hypertrophy. Provided as Drozdov_Dataset2.xls

Supplementary Tables

Supplementary Table 5. Functional enrichment of genes specific to the Pathological and Physiological networks for over-represented Gene Ontology (GO) Biological Process (BP), and Cellular Component (CC) terms, as well as Reactome pathways. inPopulation=total number of genes per term; inStudySet=number of genes in a network that mapped to a term; estimate=posterior probability estimate of functional enrichment; std.error=standard error of posterior probability estimate.

Pathological LVH				
Reactome pathway	**inPopulation**	**inStudySet**	**estimate**	**std.error**
METABOLISM::REACTOME::REACT_112621.4	1476	248	0.776	0.029
SIGNALING BY NGF::REACTOME::REACT_86675.5	227	46	0.617	0.009
CELL SURFACE INTERACTIONS AT THE VASCULAR WALL::REACTOME::REACT_86886.5	86	18	0.314	0.010
MHC CLASS II ANTIGEN PRESENTATION::REACTOME::REACT_127194.1	80	19	0.288	0.015
MEMBRANE TRAFFICKING::REACTOME::REACT_88307.5	119	24	0.287	0.016
MUSCLE CONTRACTION::REACTOME::REACT_108582.5	53	13	0.197	0.015
ACTIVATION OF GENES BY ATF4::REACTOME::REACT_131139.1	10	5	0.186	0.011
FATTY ACID, TRIACYLGLYCEROL, AND KETONE BODY METABOLISM::REACTOME::REACT_101329.5	187	39	0.176	0.023
INTEGRIN CELL SURFACE INTERACTIONS::REACTOME::REACT_100071.5	82	18	0.172	0.008
COLLAGEN BIOSYNTHESIS AND MODIFYING ENZYMES::REACTOME::REACT_138096.1	56	13	0.165	0.011
COLLAGEN FORMATION::REACTOME::REACT_131580.1	56	13	0.162	0.012
RESPONSE TO ELEVATED PLATELET CYTOSOLIC CA2+::REACTOME::REACT_32515.6	93	20	0.154	0.012
CHAPERONIN-MEDIATED PROTEIN FOLDING::REACTOME::REACT_106427.5	44	10	0.152	0.011
ELONGATION ARREST AND RECOVERY::REACTOME::REACT_82766.5	38	9	0.146	0.012
INTERLEUKIN-2 SIGNALING::REACTOME::REACT_29186.6	42	8	0.139	0.012
PERK REGULATED GENE EXPRESSION::REACTOME::REACT_108469.5	13	5	0.134	0.007
PLATELET DEGRANULATION::REACTOME::REACT_102232.5	88	19	0.128	0.006
BASIGIN INTERACTIONS::REACTOME::REACT_91519.5	27	8	0.120	0.003
THE CITRIC ACID (TCA) CYCLE AND RESPIRATORY ELECTRON TRANSPORT::REACTOME::REACT_114046.4	148	32	0.117	0.010
GOBP	**inPopulation**	**inStudySet**	**estimate**	**std.error**
SMALL MOLECULE METABOLIC PROCESS::GO::GO:0044281	1065	190	0.668	0.124

ORGAN DEVELOPMENT::GO::GO:0048513	1976	344	0.647	0.063
TISSUE DEVELOPMENT::GO::GO:0009888	998	185	0.353	0.065
ESTABLISHMENT OF PROTEIN LOCALIZATION::GO::GO:0045184	410	75	0.200	0.030
REGULATION OF APOPTOTIC PROCESS::GO::GO:0042981	1055	198	0.186	0.040
CELLULAR KETONE METABOLIC PROCESS::GO::GO:0042180	509	97	0.156	0.072
NEGATIVE REGULATION OF PROGRAMMED CELL DEATH::GO::GO:0043069	588	118	0.119	0.028
AMINE METABOLIC PROCESS::GO::GO:0009308	164	36	0.115	0.090
NEGATIVE REGULATION OF APOPTOTIC PROCESS::GO::GO:0043066	583	118	0.113	0.026
PROTEIN LOCALIZATION::GO::GO:0008104	683	112	0.112	0.062
REGULATION OF PROGRAMMED CELL DEATH::GO::GO:0043067	1065	198	0.104	0.034
BIOLOGICAL ADHESION::GO::GO:0022610	351	65	0.104	0.045
GOCC	**inPopulation**	**inStudySet**	**estimate**	**std.error**
MITOCHONDRIAL PART::GO::GO:0044429	466	110	0.941	0.003
EXTRACELLULAR REGION PART::GO::GO:0044421	799	144	0.887	0.008
SOLUBLE FRACTION::GO::GO:0005625	321	60	0.631	0.023
CAVEOLA::GO::GO:0005901	64	19	0.605	0.019
VESICULAR FRACTION::GO::GO:0042598	209	39	0.381	0.021
MICROSOME::GO::GO:0005792	204	37	0.373	0.011
LAMELLIPODIUM::GO::GO:0030027	97	20	0.340	0.009
SECRETORY GRANULE::GO::GO:0030141	222	45	0.228	0.008
MICROTUBULE ASSOCIATED COMPLEX::GO::GO:0005875	63	14	0.219	0.009
CONTRACTILE FIBER PART::GO::GO:0044449	129	25	0.201	0.004
CYTOSOLIC PART::GO::GO:0044445	154	28	0.160	0.012
NEURON PROJECTION TERMINUS::GO::GO:0044306	96	23	0.136	0.006
U12-TYPE SPLICEOSOMAL COMPLEX::GO::GO:0005689	24	7	0.115	0.003
LATE ENDOSOME MEMBRANE::GO::GO:0031902	16	6	0.114	0.005
MEMBRANE RAFT::GO::GO:0045121	217	43	0.109	0.007
NUCLEAR UBIQUITIN LIGASE COMPLEX::GO::GO:0000152	21	6	0.102	0.004
Physiological LVH				
Reactome	**inPopulation**	**inStudySet**	**estimate**	**std.error**
DEADENYLATION-DEPENDENT MRNA DECAY::REACTOME::REACT_94503.5	53	15	0.895	0.009
G ALPHA (I) SIGNALLING EVENTS::REACTOME::REACT_90291.5	185	30	0.538	0.020
NUCLEAR RECEPTOR TRANSCRIPTION PATHWAY::REACTOME::REACT_99688.5	49	11	0.535	0.015
GLUCOSE METABOLISM::REACTOME::REACT_80637.5	69	13	0.445	0.019
DOWNSTREAM SIGNAL TRANSDUCTION::REACTOME::REACT_100635.5	92	20	0.305	0.013
INTRINSIC PATHWAY FOR APOPTOSIS::REACTOME::REACT_98486.5	32	8	0.275	0.007

ACTIVATION OF CHAPERONE GENES BY ATF6-ALPHA::REACTOME::REACT_138784.1	10	5	0.269	0.008
GLUCONEOGENESIS::REACTOME::REACT_30814.6	38	9	0.236	0.016
ION CHANNEL TRANSPORT::REACTOME::REACT_94109.5	47	9	0.228	0.014
CENTROSOME MATURATION::REACTOME::REACT_96096.5	73	13	0.205	0.007
AMINO ACID SYNTHESIS AND INTERCONVERSION (TRANSAMINATION)::REACTOME::REACT_77379.5	18	6	0.205	0.006
ACTIVATION OF CHAPERONES BY ATF6-ALPHA::REACTOME::REACT_90461.5	12	5	0.199	0.020
RECRUITMENT OF MITOTIC CENTROSOME PROTEINS AND COMPLEXES::REACTOME::REACT_92567.5	73	13	0.193	0.010
TRANSPORT OF MATURE MRNA DERIVED FROM AN INTRON-CONTAINING TRANSCRIPT::REACTOME::REACT_94770.5	53	11	0.174	0.007
ACTIVATION OF BH3-ONLY PROTEINS::REACTOME::REACT_91879.5	12	5	0.153	0.008
ENDOGENOUS STEROLS::REACTOME::REACT_77256.5	14	4	0.150	0.009
ALPHA-LINOLENIC ACID (ALA) METABOLISM::REACTOME::REACT_126519.1	12	4	0.149	0.005
INTERFERON SIGNALING::REACTOME::REACT_127785.1	70	14	0.140	0.006
SIGNAL AMPLIFICATION::REACTOME::REACT_79654.5	16	5	0.138	0.012
ALPHA-LINOLENIC (OMEGA3) AND LINOLEIC (OMEGA6) ACID METABOLISM::REACTOME::REACT_142772.1	12	4	0.135	0.007
ION TRANSPORT BY P-TYPE ATPASES::REACTOME::REACT_108918.5	27	6	0.130	0.008
ACTIVATION OF THE AP-1 FAMILY OF TRANSCRIPTION FACTORS::REACTOME::REACT_99415.5	11	5	0.121	0.007
ATTACHMENT OF GPI ANCHOR TO UPAR::REACTOME::REACT_85671.5	7	3	0.119	0.006
HEXOSE UPTAKE::REACTOME::REACT_77183.5	41	8	0.112	0.008
TRANSPORT OF MATURE TRANSCRIPT TO CYTOPLASM::REACTOME::REACT_33590.6	57	11	0.104	0.006
SIGNALING BY PDGF::REACTOME::REACT_80348.5	115	22	0.102	0.011
CHOLESTEROL BIOSYNTHESIS::REACTOME::REACT_30476.6	24	5	0.101	0.004
GOBP	**inPopulation**	**inStudySet**	**estimate**	**std.error**
CYTOKINE-MEDIATED SIGNALING PATHWAY::GO::GO:0019221	141	28	0.697	0.050
MAPK CASCADE::GO::GO:0000165	136	29	0.672	0.054
RESPONSE TO REACTIVE OXYGEN SPECIES::GO::GO:0000302	86	21	0.575	0.035
ORGANIC SUBSTANCE TRANSPORT::GO::GO:0071702	285	46	0.532	0.020
GLAND DEVELOPMENT::GO::GO:0048732	238	39	0.403	0.048
REGULATION OF REPRODUCTIVE	107	18	0.192	0.013

PROCESS::GO::GO:2000241				
CELLULAR RESPONSE TO CYTOKINE STIMULUS::GO::GO:0071345	210	37	0.182	0.057
ICOSANOID METABOLIC PROCESS::GO::GO:0006690	48	12	0.174	0.019
CELLULAR MACROMOLECULE CATABOLIC PROCESS::GO::GO:0044265	294	45	0.173	0.034
PURINE RIBONUCLEOSIDE TRIPHOSPHATE CATABOLIC PROCESS::GO::GO:0009207	203	33	0.171	0.025
REGULATION OF CALCIUM ION TRANSPORT INTO CYTOSOL::GO::GO:0010522	44	13	0.164	0.036
RESPONSE TO TOXIN::GO::GO:0009636	58	17	0.157	0.029
ER TO GOLGI VESICLE-MEDIATED TRANSPORT::GO::GO:0006888	24	9	0.157	0.010
REGULATION OF RELEASE OF SEQUESTERED CALCIUM ION INTO CYTOSOL::GO::GO:0051279	30	9	0.150	0.026
GLUCOSE METABOLIC PROCESS::GO::GO:0006006	76	18	0.134	0.020
EPITHELIAL CELL DIFFERENTIATION::GO::GO:0030855	211	32	0.131	0.033
RIBONUCLEOSIDE TRIPHOSPHATE CATABOLIC PROCESS::GO::GO:0009203	204	33	0.125	0.012
UNSATURATED FATTY ACID METABOLIC PROCESS::GO::GO:0033559	50	12	0.114	0.031
ANGIOGENESIS::GO::GO:0001525	164	29	0.106	0.012
POSITIVE REGULATION OF CELL CYCLE::GO::GO:0045787	111	20	0.103	0.013
RIBONUCLEOPROTEIN COMPLEX SUBUNIT ORGANIZATION::GO::GO:0071826	74	15	0.102	0.007
CELLULAR RESPONSE TO STRESS::GO::GO:0033554	669	102	0.100	0.041
GOCC	**inPopulation**	**inStudySet**	**estimate**	**std.error**
PML BODY::GO::GO:0016605	51	12	0.883	0.008
PORE COMPLEX::GO::GO:0046930	31	9	0.594	0.020
RIBONUCLEOPROTEIN GRANULE::GO::GO:0035770	66	13	0.520	0.013
SOLUBLE FRACTION::GO::GO:0005625	321	47	0.488	0.023
VESICULAR FRACTION::GO::GO:0042598	209	34	0.383	0.030
MICROTUBULE::GO::GO:0005874	130	21	0.343	0.010
MICROSOME::GO::GO:0005792	204	33	0.303	0.011
CATALYTIC STEP 2 SPLICEOSOME::GO::GO:0071013	78	13	0.275	0.006
RUFFLE::GO::GO:0001726	88	13	0.244	0.009
CYTOPLASMIC STRESS GRANULE::GO::GO:0010494	26	7	0.237	0.008
SPINDLE MICROTUBULE::GO::GO:0005876	37	8	0.207	0.011
CELL FRACTION::GO::GO:0000267	825	115	0.198	0.033
CCAAT-BINDING FACTOR COMPLEX::GO::GO:0016602	4	3	0.193	0.007
NUCLEAR INCLUSION BODY::GO::GO:0042405	5	4	0.184	0.011
SARCOLEMMA::GO::GO:0042383	94	17	0.169	0.006
INCLUSION BODY::GO::GO:0016234	33	8	0.168	0.008
SMAD PROTEIN	4	3	0.166	0.005

COMPLEX::GO::GO:0071141				
SPLICEOSOMAL COMPLEX::GO::GO:0005681	106	16	0.162	0.008
NUCLEAR PORE::GO::GO:0005643	27	7	0.159	0.010
T-TUBULE::GO::GO:0030315	36	9	0.156	0.004
ENDOPLASMIC RETICULUM LUMEN::GO::GO:0005788	36	7	0.145	0.006
ENDOCYTIC VESICLE::GO::GO:0030139	60	11	0.143	0.007
PERINUCLEAR REGION OF CYTOPLASM::GO::GO:0048471	371	53	0.138	0.016
TRANSCRIPTIONALLY ACTIVE CHROMATIN::GO::GO:0035327	8	3	0.124	0.007
CORNIFIED ENVELOPE::GO::GO:0001533	24	5	0.123	0.005
PROTEASOME COMPLEX::GO::GO:0000502	17	5	0.121	0.005
MITOCHONDRIAL CRISTA::GO::GO:0030061	9	3	0.118	0.006
CYTOPLASMIC MRNA PROCESSING BODY::GO::GO:0000932	32	7	0.117	0.004
MULTIVESICULAR BODY::GO::GO:0005771	25	6	0.105	0.002

Supplementary Table 6. Functional enrichment of all genes specific in the Pathological and Physiological networks for over-represented Gene Ontology (GO) Biological Process (BP), and Cellular Component (CC) terms, as well as Reactome pathways. inPopulation=total number of genes per term; inStudySet=number of genes in a network that mapped to a term; estimate=posterior probability estimate of functional enrichment; std.error=standard error of posterior probability estimate

Physiological LVH

Reactome	inPopulation	inStudySet	estimate	std.error
INTERFERON SIGNALING::REACTOME::REACT_127785.1	70	29	0.914	0.007
GLUCOSE METABOLISM::REACTOME::REACT_80637.5	69	24	0.837	0.016
THE CITRIC ACID (TCA) CYCLE AND RESPIRATORY ELECTRON TRANSPORT::REACTOME::REACT_114046.4	148	46	0.760	0.012
CYTOSOLIC TRNA AMINOACYLATION::REACTOME::REACT_59282.6	27	12	0.626	0.025
NUCLEAR RECEPTOR TRANSCRIPTION PATHWAY::REACTOME::REACT_99688.5	49	20	0.593	0.013
ANTIGEN PROCESSING: UBIQUITINATION & PROTEASOME DEGRADATION::REACTOME::REACT_131037.1	64	29	0.517	0.016
SIGNALING BY PDGF::REACTOME::REACT_80348.5	115	47	0.483	0.012
NCAM1 INTERACTIONS::REACTOME::REACT_86877.5	34	17	0.466	0.006
BRANCHED-CHAIN AMINO ACID CATABOLISM::REACTOME::REACT_32990.6	17	9	0.392	0.017
MITOCHONDRIAL PROTEIN IMPORT::REACTOME::REACT_144481.1	47	15	0.363	0.016
MUSCLE CONTRACTION::REACTOME::REACT_108582.5	53	18	0.359	0.009
DEADENYLATION-DEPENDENT MRNA DECAY::REACTOME::REACT_94503.5	53	19	0.329	0.012
MEMBRANE TRAFFICKING::REACTOME::REACT_88307.5	119	35	0.317	0.019
DEADENYLATION OF MRNA::REACTOME::REACT_56462.6	26	12	0.293	0.008
GENERIC TRANSCRIPTION PATHWAY::REACTOME::REACT_85098.5	141	42	0.276	0.017
CIRCADIAN CLOCK::REACTOME::REACT_109335.5	55	19	0.266	0.010
PLATELET AGGREGATION (PLUG FORMATION)::REACTOME::REACT_90514.5	37	15	0.260	0.010
CATION-COUPLED CHLORIDE COTRANSPORTERS::REACTOME::REACT_81104.5	7	5	0.248	0.010
APOPTOSIS::REACTOME::REACT_100962.5	140	48	0.238	0.013
ATTACHMENT OF GPI ANCHOR TO UPAR::REACTOME::REACT_85671.5	7	5	0.228	0.014
INWARDLY RECTIFYING K+ CHANNELS::REACTOME::REACT_108208.5	36	13	0.223	0.008

TRANSPORT OF MATURE MRNA DERIVED FROM AN INTRON-CONTAINING TRANSCRIPT::REACTOME::REACT_94770.5	53	20	0.211	0.012
SIGNALING BY EGFR::REACTOME::REACT_82411.5	109	40	0.207	0.009
LATENT INFECTION OF HOMO SAPIENS WITH MYCOBACTERIUM TUBERCULOSIS::REACTOME::REACT_146901.1	32	12	0.205	0.012
PERK REGULATED GENE EXPRESSION::REACTOME::REACT_108469.5	13	7	0.204	0.003
MHC CLASS II ANTIGEN PRESENTATION::REACTOME::REACT_127194.1	80	27	0.196	0.012
PHAGOSOMAL MATURATION (EARLY ENDOSOMAL STAGE)::REACTOME::REACT_126778.1	32	12	0.187	0.007
SIGNALING BY EGFR IN CANCER::REACTOME::REACT_118233.3	111	41	0.183	0.007
MITOTIC METAPHASE ANAPHASE TRANSITION::REACTOME::REACT_88639.5	7	5	0.177	0.004
INSULIN RECEPTOR RECYCLING::REACTOME::REACT_81379.5	25	10	0.166	0.011
ACTIVATION OF CHAPERONE GENES BY ATF6-ALPHA::REACTOME::REACT_138784.1	10	6	0.166	0.005
ATP SENSITIVE POTASSIUM CHANNELS::REACTOME::REACT_147052.1	4	4	0.161	0.009
ALPHA-LINOLENIC (OMEGA3) AND LINOLEIC (OMEGA6) ACID METABOLISM::REACTOME::REACT_142772.1	12	6	0.157	0.006
TRAFFICKING AND PROCESSING OF ENDOSOMAL TLR::REACTOME::REACT_129583.1	12	6	0.153	0.006
DOWNSTREAM SIGNAL TRANSDUCTION::REACTOME::REACT_100635.5	92	36	0.152	0.010
ALPHA-LINOLENIC ACID (ALA) METABOLISM::REACTOME::REACT_126519.1	12	6	0.151	0.010
PI METABOLISM::REACTOME::REACT_144613.1	48	16	0.144	0.012
RECRUITMENT OF MITOTIC CENTROSOME PROTEINS AND COMPLEXES::REACTOME::REACT_92567.5	73	24	0.143	0.006
STRIATED MUSCLE CONTRACTION::REACTOME::REACT_88644.5	28	10	0.138	0.007
GOLGI TO ER RETROGRADE TRANSPORT::REACTOME::REACT_78992.5	10	6	0.136	0.005
MITOTIC G2-G2 M PHASES::REACTOME::REACT_105104.5	88	28	0.136	0.005
ENDOSOMAL SORTING COMPLEX REQUIRED FOR TRANSPORT (ESCRT)::REACTOME::REACT_141747.1	28	10	0.135	0.018
COPI MEDIATED TRANSPORT::REACTOME::REACT_80406.	10	6	0.135	0.006

5				
G2 M TRANSITION::REACTOME::REACT_34062.6	85	27	0.130	0.009
CENTROSOME MATURATION::REACTOME::REACT_96096.5	73	24	0.130	0.007
INHIBITION OF REPLICATION INITIATION OF DAMAGED DNA BY RB1 E2F1::REACTOME::REACT_82590.5	6	5	0.128	0.005
INHIBITION OF INSULIN SECRETION BY ADRENALINE NORADRENALINE::REACTOME::REACT_86915.5	34	13	0.127	0.006
CREATINE METABOLISM::REACTOME::REACT_106712.5	7	4	0.120	0.003
INTRINSIC PATHWAY FOR APOPTOSIS::REACTOME::REACT_98486.5	32	12	0.120	0.008
CLEAVAGE OF GROWING TRANSCRIPT IN THE TERMINATION REGION::REACTOME::REACT_92795.5	47	17	0.118	0.006
E2F MEDIATED REGULATION OF DNA REPLICATION::REACTOME::REACT_104779.5	27	10	0.117	0.003
REGULATION OF GENE EXPRESSION BY HYPOXIA-INDUCIBLE FACTOR::REACTOME::REACT_137830.1	9	5	0.115	0.007
NCAM SIGNALING FOR NEURITE OUT-GROWTH::REACTOME::REACT_88653.5	60	26	0.114	0.008
POST-ELONGATION PROCESSING OF THE TRANSCRIPT::REACTOME::REACT_105197.5	47	17	0.114	0.005
PYRUVATE METABOLISM AND CITRIC ACID (TCA) CYCLE::REACTOME::REACT_80935.5	40	16	0.113	0.008
SYNTHESIS OF PIPS AT THE PLASMA MEMBRANE::REACTOME::REACT_140792.1	31	11	0.109	0.007
RNA POLYMERASE II TRANSCRIPTION TERMINATION::REACTOME::REACT_33376.6	47	17	0.107	0.005
DCC MEDIATED ATTRACTIVE SIGNALING::REACTOME::REACT_93929.5	14	6	0.106	0.004
LOSS OF PROTEINS REQUIRED FOR INTERPHASE MICROTUBULE ORGANIZATIONåÊFROM THE CENTROSOME::REACTOME::REACT_106686.5	63	21	0.105	0.002
DOWNREGULATION OF SMAD2 3:SMAD4 TRANSCRIPTIONAL ACTIVITY::REACTOME::REACT_141912.1	26	9	0.104	0.006

GOBP	**inPopulation**	**inStudySet**	**estimate**	**std.error**
INTRACELLULAR TRANSPORT%GO%GO:0046907	544	155	0.572	0.214
REGULATION OF BIOLOGICAL QUALITY%GO%GO:0065008	1766	415	0.373	0.198
METABOLIC PROCESS%GO%GO:0008152	4430	1033	0.371	0.228
NEGATIVE REGULATION OF PROTEIN METABOLIC PROCESS%GO%GO:0051248	371	110	0.354	0.146
POSITIVE REGULATION OF METABOLIC PROCESS%GO%GO:0009893	1800	455	0.348	0.175
CATABOLIC PROCESS%GO%GO:0009056	927	271	0.347	0.159

PROGRAMMED CELL DEATH%GO%GO:0012501	417	131	0.324	0.053
TISSUE MORPHOGENESIS%GO%GO:0048729	445	124	0.324	0.107
LOCALIZATION%GO%GO:0051179	2335	535	0.271	0.172
REGULATION OF RESPONSE TO STIMULUS%GO%GO:0048583	1796	426	0.245	0.144
BLOOD CIRCULATION%GO%GO:0008015	218	66	0.231	0.093
CELLULAR CATABOLIC PROCESS%GO%GO:0044248	808	239	0.208	0.117
COENZYME METABOLIC PROCESS%GO%GO:0006732	145	50	0.199	0.082
PROTEIN HETEROOLIGOMERIZATION%GO%GO:0051291	92	34	0.199	0.073
RESPONSE TO METAL ION%GO%GO:0010038	151	54	0.187	0.076
REGULATION OF MOLECULAR FUNCTION%GO%GO:0065009	1590	356	0.185	0.116
POSITIVE REGULATION OF CELLULAR PROCESS%GO%GO:0048522	2901	698	0.184	0.087
COFACTOR METABOLIC PROCESS%GO%GO:0051186	176	56	0.176	0.073
APOPTOTIC PROCESS%GO%GO:0006915	402	126	0.176	0.052
REGULATION OF RNA SPLICING%GO%GO:0043484	58	25	0.174	0.071
REGULATION OF PRIMARY METABOLIC PROCESS%GO%GO:0080090	2980	689	0.169	0.118
CELL DEATH%GO%GO:0008219	465	141	0.169	0.038
INTRACELLULAR SIGNAL TRANSDUCTION%GO%GO:0035556	645	166	0.167	0.103
CELLULAR COMPONENT ORGANIZATION%GO%GO:0016043	2581	577	0.166	0.122
RIBONUCLEOPROTEIN COMPLEX ASSEMBLY%GO%GO:0022618	70	27	0.166	0.068
CIRCULATORY SYSTEM PROCESS%GO%GO:0003013	219	66	0.158	0.064
REGULATION OF CELLULAR METABOLIC PROCESS%GO%GO:0031323	3024	699	0.140	0.106
EMBRYO DEVELOPMENT ENDING IN BIRTH OR EGG HATCHING%GO%GO:0009792	558	151	0.130	0.053
RIBONUCLEOPROTEIN COMPLEX SUBUNIT ORGANIZATION%GO%GO:0071826	74	28	0.118	0.054
LOCOMOTION%GO%GO:0040011	659	152	0.118	0.097
POSITIVE REGULATION OF RESPONSE TO STIMULUS%GO%GO:0048584	918	234	0.109	0.068
CELL-CELL SIGNALING%GO%GO:0007267	458	100	0.109	0.047
EPITHELIUM DEVELOPMENT%GO%GO:0060429	492	136	0.107	0.042

GOCC	**inPopulation**	**inStudySet**	**estimate**	**std.error**
CELL-CELL JUNCTION%GO%GO:0005911	243	54	0.648	0.095
EXTRACELLULAR REGION PART%GO%GO:0044421	799	180	0.527	0.079
EXTRACELLULAR MATRIX%GO%GO:0031012	238	60	0.506	0.055
CELL PART%GO%GO:0044464	10091	2203	0.479	0.071
POSTSYNAPTIC MEMBRANE%GO%GO:0045211	69	19	0.414	0.046
CELL%GO%GO:0005623	10093	2203	0.330	0.055

EXTRACELLULAR SPACE%GO%GO:0005615	652	152	0.285	0.046
ORGANELLE MEMBRANE%GO%GO:0031090	956	249	0.246	0.079
CYTOSOL%GO%GO:0005829	932	264	0.196	0.115
ENDOSOME%GO%GO:0005768	340	100	0.174	0.107
NUCLEUS%GO%GO:0005634	3979	927	0.161	0.104
MEPRIN A COMPLEX%GO%GO:0017090	1	1	0.144	0.017
CELL JUNCTION%GO%GO:0030054	382	90	0.137	0.032
PROTEIN COMPLEX%GO%GO:0043234	2337	588	0.125	0.020
SYNAPTIC MEMBRANE%GO%GO:0097060	103	26	0.123	0.026
SARCOLEMMA%GO%GO:0042383	94	37	0.121	0.074
SYNAPSE%GO%GO:0045202	427	91	0.121	0.024
ORGANELLE PART%GO%GO:0044422	3721	898	0.118	0.020
MEMBRANE-BOUNDED ORGANELLE%GO%GO:0043227	6708	1565	0.109	0.018
SYNAPSE PART%GO%GO:0044456	293	59	0.105	0.018

Pathological LVH

Reactome	inPopulation	inStudySet	estimate	std.error
MHC CLASS II ANTIGEN PRESENTATION::REACTOME::REACT_127194.1	80	41	0.997	0.002
MITOCHONDRIAL PROTEIN IMPORT::REACTOME::REACT_144481.1	47	20	0.972	0.005
THE CITRIC ACID (TCA) CYCLE AND RESPIRATORY ELECTRON TRANSPORT::REACTOME::REACT_114046.4	148	69	0.944	0.014
FATTY ACID, TRIACYLGLYCEROL, AND KETONE BODY METABOLISM::REACTOME::REACT_101329.5	187	69	0.937	0.007
GLUCOSE METABOLISM::REACTOME::REACT_80637.5	69	30	0.867	0.018
AMINO ACID AND DERIVATIVE METABOLISM::REACTOME::REACT_33347.6	196	78	0.773	0.040
CELL SURFACE INTERACTIONS AT THE VASCULAR WALL::REACTOME::REACT_86886.5	86	33	0.545	0.021
MUSCLE CONTRACTION::REACTOME::REACT_108582.5	53	24	0.537	0.029
DEVELOPMENTAL BIOLOGY::REACTOME::REACT_115492.4	387	127	0.495	0.023
PLATELET DEGRANULATION::REACTOME::REACT_102232.5	88	40	0.479	0.036
COLLAGEN FORMATION::REACTOME::REACT_131580.1	56	26	0.442	0.037
CIRCADIAN CLOCK::REACTOME::REACT_109335.5	55	23	0.433	0.007
STRIATED MUSCLE CONTRACTION::REACTOME::REACT_88644.5	28	14	0.429	0.027
PRE-MRNA SPLICING::REACTOME::REACT_95764.5	129	42	0.391	0.041

ELONGATION ARREST AND RECOVERY::REACTOME::REACT_82766.5	38	15	0.388	0.023
COLLAGEN BIOSYNTHESIS AND MODIFYING ENZYMES::REACTOME::REACT_138096.1	56	26	0.385	0.038
MRNA SPLICING::REACTOME::REACT_98753.5	129	42	0.375	0.014
CHAPERONIN-MEDIATED PROTEIN FOLDING::REACTOME::REACT_106427.5	44	18	0.370	0.026
MEMBRANE TRAFFICKING::REACTOME::REACT_88307.5	119	44	0.356	0.015
INTEGRATION OF ENERGY METABOLISM::REACTOME::REACT_105810.5	129	39	0.348	0.015
PERK REGULATED GENE EXPRESSION::REACTOME::REACT_108469.5	13	8	0.346	0.009
LATENT INFECTION OF HOMO SAPIENS WITH MYCOBACTERIUM TUBERCULOSIS::REACTOME::REACT_146901.1	32	15	0.344	0.018
RESPONSE TO ELEVATED PLATELET CYTOSOLIC CA2+::REACTOME::REACT_32515.6	93	41	0.307	0.043
PHAGOSOMAL MATURATION (EARLY ENDOSOMAL STAGE)::REACTOME::REACT_126778.1	32	15	0.307	0.015
GENERIC TRANSCRIPTION PATHWAY::REACTOME::REACT_85098.5	141	43	0.290	0.014
TRNA AMINOACYLATION::REACTOME::REACT_78082.5	45	16	0.279	0.010
PHASE II CONJUGATION::REACTOME::REACT_87608.5	59	19	0.264	0.013
CYTOSOLIC TRNA AMINOACYLATION::REACTOME::REACT_59282.6	27	11	0.263	0.014
PROTEIN FOLDING::REACTOME::REACT_106260.5	49	19	0.257	0.023
NGF PROCESSING::REACTOME::REACT_83522.5	13	6	0.254	0.012
ACTIVATION OF GENES BY ATF4::REACTOME::REACT_131139.1	10	6	0.251	0.020
COOPERATION OF PREFOLDIN AND TRIC CCT IN ACTIN AND TUBULIN FOLDING::REACTOME::REACT_96856.5	31	14	0.249	0.007
HEME BIOSYNTHESIS::REACTOME::REACT_98585.5	9	6	0.234	0.019
INTERFERON SIGNALING::REACTOME::REACT_127785.1	70	23	0.214	0.008
PLATELET ACTIVATION, SIGNALING AND AGGREGATION::REACTOME::REACT_103583.5	197	70	0.209	0.020
CS DS DEGRADATION::REACTOME::REACT_145805.1	13	7	0.195	0.011
KERATAN SULFATE DEGRADATION::REACTOME::REACT_143490.1	11	6	0.188	0.014
REGULATION OF INSULIN SECRETION::REACTOME::REACT_88056.5	101	32	0.164	0.009

PI3K EVENTS IN ERBB4 SIGNALING::REACTOME::REACT_118344.3	34	14	0.164	0.005
BRANCHED-CHAIN AMINO ACID CATABOLISM::REACTOME::REACT_32990.6	17	10	0.158	0.027
L1CAM INTERACTIONS::REACTOME::REACT_101259.5	81	33	0.150	0.021
SYNTHESIS AND INTERCONVERSION OF NUCLEOTIDE DI- AND TRIPHOSPHATES::REACTOME::REACT_82335.5	18	8	0.149	0.006
INSULIN RECEPTOR RECYCLING::REACTOME::REACT_81379.5	25	12	0.145	0.007
POST NMDA RECEPTOR ACTIVATION EVENTS::REACTOME::REACT_111033.5	33	16	0.140	0.005
HYALURONAN METABOLISM::REACTOME::REACT_145024.1	13	6	0.138	0.005
REGULATION OF WATER BALANCE BY RENAL AQUAPORINS::REACTOME::REACT_97951.5	47	17	0.135	0.012
CREB PHOSPHORYLATION THROUGH THE ACTIVATION OF CAMKII::REACTOME::REACT_145749.1	16	10	0.129	0.006
INTERLEUKIN-2 SIGNALING::REACTOME::REACT_29186.6	42	15	0.129	0.005
REGULATION OF COMPLEMENT CASCADE::REACTOME::REACT_144679.1	14	6	0.125	0.006
CATION-COUPLED CHLORIDE COTRANSPORTERS::REACTOME::REACT_81104.5	7	4	0.125	0.008
BASIGIN INTERACTIONS::REACTOME::REACT_91519.5	27	12	0.123	0.008
HYALURONAN UPTAKE AND DEGRADATION::REACTOME::REACT_131431.1	10	5	0.120	0.008
TRANSFERRIN ENDOCYTOSIS AND RECYCLING::REACTOME::REACT_146500.1	27	12	0.117	0.007
SIGNALING BY NGF::REACTOME::REACT_86675.5	227	73	0.114	0.008
GAP JUNCTION TRAFFICKING AND REGULATION::REACTOME::REACT_98857.5	13	10	0.112	0.004
RAS ACTIVATION UOPN CA2+ INFUX THROUGH NMDA RECEPTOR::REACTOME::REACT_141113.1	17	10	0.112	0.015
UNBLOCKING OF NMDA RECEPTOR, GLUTAMATE BINDING AND ACTIVATION::REACTOME::REACT_84448.5	16	8	0.111	0.009
GLUTATHIONE CONJUGATION::REACTOME::REACT_28985.6	20	7	0.111	0.011
ACTIVATION OF NMDA RECEPTOR UPON GLUTAMATE BINDING AND POSTSYNAPTIC EVENTS::REACTOME::REACT_109325.5	37	17	0.109	0.005
GLYCOLYSIS::REACTOME::REACT_96470.5	35	15	0.108	0.012
CREB PHOSPHORYLATION THROUGH THE ACTIVATION OF	27	13	0.105	0.004

RAS::REACTOME::REACT_130630.1				
NGF SIGNALLING VIA TRKA FROM THE PLASMA MEMBRANE::REACTOME::REACT_91043.5	135	50	0.102	0.010
REGULATION OF GENE EXPRESSION BY HYPOXIA-INDUCIBLE FACTOR::REACTOME::REACT_137830.1	9	6	0.101	0.008
INTERLEUKIN RECEPTOR SHC SIGNALING::REACTOME::REACT_76978.5	28	10	0.100	0.006

GOBP	**inPopulation**	**inStudySet**	**estimate**	**std.error**
POSITIVE REGULATION OF CELLULAR PROCESS%GO%GO:0048522	2901	796	0.892	0.039
METABOLIC PROCESS%GO%GO:0008152	4430	1138	0.780	0.067
CELL-CELL SIGNALING%GO%GO:0007267	458	124	0.651	0.040
CELLULAR COMPONENT ORGANIZATION%GO%GO:0016043	2581	670	0.510	0.096
INTRACELLULAR TRANSPORT%GO%GO:0046907	544	163	0.503	0.029
TISSUE DEVELOPMENT%GO%GO:0009888	998	308	0.496	0.085
CELLULAR COMPONENT ORGANIZATION OR BIOGENESIS%GO%GO:0071840	2647	680	0.315	0.083
REGULATION OF BIOLOGICAL QUALITY%GO%GO:0065008	1766	487	0.296	0.043
NEGATIVE REGULATION OF NITROGEN COMPOUND METABOLIC PROCESS%GO%GO:0051172	897	265	0.252	0.030
CELLULAR LOCALIZATION%GO%GO:0051641	1007	266	0.223	0.022
EPITHELIUM DEVELOPMENT%GO%GO:0060429	492	155	0.220	0.070
NEGATIVE REGULATION OF RNA METABOLIC PROCESS%GO%GO:0051253	821	241	0.187	0.028
REGULATION OF RNA METABOLIC PROCESS%GO%GO:0051252	1841	503	0.181	0.065
APOPTOTIC PROCESS%GO%GO:0006915	402	134	0.175	0.041
IMMUNE SYSTEM PROCESS%GO%GO:0002376	888	237	0.173	0.027
NEGATIVE REGULATION OF APOPTOTIC PROCESS%GO%GO:0043066	583	193	0.157	0.038
ESTABLISHMENT OF PROTEIN LOCALIZATION%GO%GO:0045184	410	136	0.156	0.029
NEGATIVE REGULATION OF NUCLEOBASE-CONTAINING COMPOUND METABOLIC PROCESS%GO%GO:0045934	884	258	0.139	0.022
NEGATIVE REGULATION OF CELLULAR METABOLIC PROCESS%GO%GO:0031324	1209	351	0.135	0.020
CATABOLIC PROCESS%GO%GO:0009056	927	285	0.133	0.068
ESTABLISHMENT OF LOCALIZATION IN CELL%GO%GO:0051649	786	218	0.128	0.043
SMALL MOLECULE METABOLIC PROCESS%GO%GO:0044281	1065	333	0.113	0.047
NEGATIVE REGULATION OF CELL DEATH%GO%GO:0060548	615	200	0.111	0.029
NEGATIVE REGULATION OF PROGRAMMED CELL DEATH%GO%GO:0043069	588	194	0.104	0.016
PROTEIN TRANSPORT%GO%GO:0015031	387	127	0.102	0.018

GOCC	**inPopulation**	**inStudySet**	**estimate**	**std.error**

CELL FRACTION%GO%GO:0000267	825	257	0.718	0.180
CYTOSOL%GO%GO:0005829	932	286	0.633	0.222
MITOCHONDRIAL PART%GO%GO:0044429	466	198	0.627	0.220
SPLICEOSOMAL COMPLEX%GO%GO:0005681	106	39	0.578	0.202
TRANSCRIPTION FACTOR COMPLEX%GO%GO:0005667	314	87	0.494	0.176
EXTRACELLULAR REGION PART%GO%GO:0044421	799	242	0.437	0.136
NUCLEAR UBIQUITIN LIGASE COMPLEX%GO%GO:0000152	21	11	0.349	0.126
ENDOPLASMIC RETICULUM-GOLGI INTERMEDIATE COMPARTMENT%GO%GO:0005793	36	16	0.294	0.107
EXTRACELLULAR MATRIX%GO%GO:0031012	238	85	0.269	0.107
MYOFIBRIL%GO%GO:0030016	140	51	0.265	0.097
STRESS FIBER%GO%GO:0001725	53	24	0.242	0.085
PROTEASOME COMPLEX%GO%GO:0000502	17	8	0.238	0.082
CONTRACTILE FIBER%GO%GO:0043292	153	55	0.233	0.079
CYTOPLASMIC MICROTUBULE%GO%GO:0005881	25	10	0.202	0.073
POLYSOME%GO%GO:0005844	27	10	0.202	0.070
EXTRINSIC TO PLASMA MEMBRANE%GO%GO:0019897	71	29	0.198	0.064
MICROTUBULE ASSOCIATED COMPLEX%GO%GO:0005875	63	20	0.191	0.067
CAVEOLA%GO%GO:0005901	64	26	0.185	0.064
PEROXISOMAL PART%GO%GO:0044439	53	21	0.175	0.060
ACTIN FILAMENT BUNDLE%GO%GO:0032432	56	24	0.174	0.064
LATE ENDOSOME%GO%GO:0005770	106	37	0.172	0.061
MEMBRANE RAFT%GO%GO:0045121	217	74	0.169	0.062
INTRACELLULAR%GO%GO:0005622	8779	2227	0.161	0.161
EXTRINSIC TO MEMBRANE%GO%GO:0019898	96	34	0.161	0.052
SIGNALOSOME%GO%GO:0008180	9	6	0.160	0.056
MICROBODY PART%GO%GO:0044438	53	21	0.158	0.056
SYNAPSE%GO%GO:0045202	427	110	0.148	0.148
CELL JUNCTION%GO%GO:0030054	382	102	0.142	0.142
APICAL PART OF CELL%GO%GO:0045177	296	86	0.140	0.104
CELL SURFACE%GO%GO:0009986	550	161	0.138	0.137
INTERNAL SIDE OF PLASMA MEMBRANE%GO%GO:0009898	90	33	0.134	0.047
COATED MEMBRANE%GO%GO:0048475	35	13	0.122	0.041
MEMBRANE COAT%GO%GO:0030117	35	13	0.120	0.040
ANAPHASE-PROMOTING COMPLEX%GO%GO:0005680	17	9	0.116	0.038
INTRINSIC TO MEMBRANE%GO%GO:0031224	2162	223	0.107	0.107
CORTICAL CYTOSKELETON%GO%GO:0030863	60	20	0.106	0.036
LATE ENDOSOME MEMBRANE%GO%GO:0031902	16	9	0.101	0.033

Supplementary Table S8. Functional enrichment of genes in the top 25th percentile of differential wiring for over-represented Gene Ontology (GO) Biological Process (BP), and Cellular Component (CC) terms, as well as Reactome pathways. inPopulation=total number of genes per term; inStudySet=number of genes in a network that mapped to a term; estimate=posterior probability estimate of functional enrichment; std.error=standard error of posterior probability estimate

Reactome	**inPopulation**	**inStudySet**	**estimate**	**std.error**
BRANCHED-CHAIN AMINO ACID CATABOLISM::REACTOME::REACT_32990.6	17	6	0.712	0.027
GOBP	**inPopulation**	**inStudySet**	**estimate**	**std.error**
MYELIN ASSEMBLY%GO%GO:0032288	11	4	0.921	0.035
HYDROGEN PEROXIDE METABOLIC PROCESS%GO%GO:0042743	25	5	0.624	0.059
COENZYME METABOLIC PROCESS%GO%GO:0006732	145	13	0.618	0.076
MRNA SPLICE SITE SELECTION%GO%GO:0006376	12	4	0.617	0.073
NEGATIVE REGULATION OF TRANSLATIONAL INITIATION%GO%GO:0045947	12	3	0.438	0.035
PROTEIN LOCALIZATION IN MITOCHONDRION%GO%GO:0070585	27	4	0.376	0.044
POSITIVE REGULATION OF MACROAUTOPHAGY%GO%GO:0016239	10	3	0.322	0.057
REGULATION OF MUSCLE ADAPTATION%GO%GO:0043502	27	4	0.313	0.028
REGULATION OF VASCULAR ENDOTHELIAL GROWTH FACTOR RECEPTOR SIGNALING PATHWAY%GO%GO:0030947	23	4	0.269	0.046
SPLICEOSOMAL COMPLEX ASSEMBLY%GO%GO:0000245	19	4	0.264	0.060
GOCC	**inPopulation**	**inStudySet**	**estimate**	**std.error**
NA	NA	NA	NA	NA

References

1. Parkinson H, Kapushesky M, Kolesnikov N, Rustici G, Shojatalab M, Abeygunawardena N, et al. Arrayexpress update--from an archive of functional genomics experiments to the atlas of gene expression. *Nucleic Acids Res*. 2009;37:D868-872
2. Irizarry RA, Hobbs B, Collin F, Beazer-Barclay YD, Antonellis KJ, Scherf U, et al. Exploration, normalization, and summaries of high density oligonucleotide array probe level data. *Biostatistics*. 2003;4:249-264
3. Gautier L, Cope L, Bolstad BM, Irizarry RA. Affy--analysis of affymetrix genechip data at the probe level. *Bioinformatics*. 2004;20:307-315
4. Maglott D, Ostell J, Pruitt KD, Tatusova T. Entrez gene: Gene-centered information at ncbi. *Nucleic acids research*. 2011;39:D52-57
5. Miller JA, Horvath S, Geschwind DH. Divergence of human and mouse brain transcriptome highlights alzheimer disease pathways. *Proc Natl Acad Sci U S A*. 2010;107:12698-12703
6. Reverter A, Chan EK. Combining partial correlation and an information theory approach to the reversed engineering of gene co-expression networks. *Bioinformatics*. 2008;24:2491-2497
7. Basso K, Margolin AA, Stolovitzky G, Klein U, Dalla-Favera R, Califano A. Reverse engineering of regulatory networks in human b cells. *Nat Genet*. 2005;37:382-390
8. Magwene PM, Kim J. Estimating genomic coexpression networks using first-order conditional independence. *Genome Biol*. 2004;5:R100
9. Maslov S, Sneppen K. Specificity and stability in topology of protein networks. *Science*. 2002;296:910-913
10. Jeong H, Mason SP, Barabasi AL, Oltvai ZN. Lethality and centrality in protein networks. *Nature*. 2001;411:41-42
11. Yu H, Kim PM, Sprecher E, Trifonov V, Gerstein M. The importance of bottlenecks in protein networks: Correlation with gene essentiality and expression dynamics. *PLoS Comput Biol*. 2007;3:e59
12. Lohmann G, Margulies DS, Horstmann A, Pleger B, Lepsien J, Goldhahn D, et al. Eigenvector centrality mapping for analyzing connectivity patterns in fmri data of the human brain. *PLoS One*. 2010;5:e10232
13. Feldman I, Rzhetsky A, Vitkup D. Network properties of genes harboring inherited disease mutations. *Proceedings of the National Academy of Sciences of the United States of America*. 2008;105:4323-4328
14. Arita M. The metabolic world of escherichia coli is not small. *Proc Natl Acad Sci U S A*. 2004;101:1543-1547
15. Travers J, Milgram S. An experimental study of the small world problem. *Sociometry*. 1969;32:425-443
16. Wuchty S, Almaas E. Peeling the yeast protein network. *Proteomics*. 2005;5:444-449
17. Clauset A, Newman MEJ, Moore C. Finding community structure in very large networks. *Phys. Rev. E*. 2004;70
18. Newman ME. Modularity and community structure in networks. *Proc Natl Acad Sci U S A*. 2006;103:8577-8582
19. Drozdov I, Ouzounis CA, Shah AM, Tsoka S. Functional genomics assistant (fuga): A toolbox for the analysis of complex biological networks. *BMC Res Notes*. 2011;4:462
20. Csárdi G, Nepusz T. The igraph software package for complex network research. *InterJournal Complex Systems*. 2006:1695
21. Weng MP, Liao BY. Mamphea: A web tool for mammalian phenotype enrichment analysis. *Bioinformatics*. 2010;26:2212-2213
22. Huang da W, Sherman BT, Lempicki RA. Bioinformatics enrichment tools: Paths toward the comprehensive functional analysis of large gene lists. *Nucleic Acids Res*. 2009;37:1-13

23. Matthews L, Gopinath G, Gillespie M, Caudy M, Croft D, de Bono B, et al. Reactome knowledgebase of human biological pathways and processes. *Nucleic Acids Res*. 2009;37:D619-622
24. Bauer S, Robinson PN, Gagneur J. Model-based gene set analysis for bioconductor. *Bioinformatics*. 2011;27:1882-1883
25. Subramanian A, Tamayo P, Mootha VK, Mukherjee S, Ebert BL, Gillette MA, et al. Gene set enrichment analysis: A knowledge-based approach for interpreting genome-wide expression profiles. *Proc Natl Acad Sci U S A*. 2005;102:15545-15550
26. Hu P, Zhang D, Swenson L, Chakrabarti G, Abel ED, Litwin SE. Minimally invasive aortic banding in mice: Effects of altered cardiomyocyte insulin signaling during pressure overload. *Am J Physiol Heart Circ Physiol*. 2003;285:H1261-1269
27. De Bono JP, Adlam D, Paterson DJ, Channon KM. Novel quantitative phenotypes of exercise training in mouse models. *Am J Physiol Regul Integr Comp Physiol*. 2006;290:R926-934
28. Byrne JA, Grieve DJ, Bendall JK, Li JM, Gove C, Lambeth JD, et al. Contrasting roles of nadph oxidase isoforms in pressure-overload versus angiotensin ii-induced cardiac hypertrophy. *Circ Res*. 2003;93:802-805
29. Didangelos A, Yin X, Mandal K, Baumert M, Jahangiri M, Mayr M. Proteomics characterization of extracellular space components in the human aorta. *Mol Cell Proteomics*. 2010;9:2048-2062
30. Waanders LF, Almeida R, Prosser S, Cox J, Eikel D, Allen MH, et al. A novel chromatographic method allows on-line reanalysis of the proteome. *Mol Cell Proteomics*. 2008;7:1452-1459
31. Keller A, Nesvizhskii AI, Kolker E, Aebersold R. Empirical statistical model to estimate the accuracy of peptide identifications made by ms/ms and database search. *Anal Chem*. 2002;74:5383-5392
32. Nesvizhskii AI, Keller A, Kolker E, Aebersold R. A statistical model for identifying proteins by tandem mass spectrometry. *Anal Chem*. 2003;75:4646-4658
33. Smyth GK. Limma: Linear models for microarray data. In: R. Gentleman VC, S. Dudoit, R. Irizarry, W. Huber, ed. *Bioinformatics and computational biology solutions using r and bioconductor*. New York: Springer; 2005:397–420.
34. Merico D, Isserlin R, Stueker O, Emili A, Bader GD. Enrichment map: A network-based method for gene-set enrichment visualization and interpretation. *PLoS One*. 2010;5:e13984.